Journal of South American Earth Sciences 52 (2014) 179–193

Contents lists available at ScienceDirect

Journal of South American Earth Sciences

journal homepage: www.elsevier.com/locate/jsames

# Provenance of the Eocene Soebi Blanco formation, Bonaire, Leeward Antilles: Correlations with post-Eocene tectonic evolution of northern South America

S. Zapata [a,f,*], A. Cardona [b], C. Montes [c], V. Valencia [d], J. Vervoort [d], P. Reiners [e]

[a] Corporación Geológica Ares, Calle 44a, #53-96, Bogota, Colombia
[b] Departamento de Procesos y Energía, Universidad Nacional de Colombia Sede Medellín, Colombia
[c] Departamento de Geociencias, Universidad de Los Andes, Bogota, Colombia, USA
[d] School of Earth and Environmental Sciences, Washington State University, Pullman, WA, USA
[e] Department of Geosciences, University of Arizona, Tucson, AZ, USA
[f] Smithsonian Tropical Research Institute, Colombia

ARTICLE INFO

*Article history:*
Received 8 October 2013
Accepted 28 February 2014

*Keywords:*
Provenance
Caribbean plate
Conglomerates
Leeward Antilles
Paleogeography

ABSTRACT

Middle to upper Eocene fluvial strata in the island of Bonaire contain detrital components that were tracked to Precambrian to Triassic massifs in northern Colombia and Venezuela. These detrital components confirm previous hypothesis suggesting that Bonaire and the Leeward Antilles were attached to South American basement massifs (SABM). These are composed of different fragmented South American blocks (Paraguana, Falcon, Maracaibo, Guajira, Perija, and Santa Marta) representing an Eocene, right-laterally displaced tectonic piercing point along the southern Caribbean plate margin. U–Pb LA-ICP-MS from the metamorphic boulders of the Soebi Blanco Formation in Bonaire yield Grenvillian peaks ages (1000–1200 Ma), while detrital zircons recovered from the sandy matrix of the conglomerates contain populations with peaks of 1000 Ma–1200 Ma, 750–950 Ma, and 200–300 Ma. These populations match with geochronological data reported for the northern South American massifs. Thermochronological results from the metamorphic clasts yield Paleocene–middle Eocene ages (65–50 Ma) that confirm a regional-scale cooling event in this time. These data imply a land connection between the SABM and the Leeward Antilles in late Eocene times, followed by a significant strike slip right-lateral displacement and transtensional basin opening starting in latest Eocene times. The succession of Eocene tectonic events recorded by the Soebi Blanco Formation and adjacent basins is a major tracer of the oblique convergence of the Caribbean plate against the South American margin.



## 1. Introduction

Oblique convergent margins are characterized by strike slip displacement of crustal segments that commonly destroy the lateral continuity of formed orogenic belts, forming isolated crustal blocks separated by extensional basins (Cowan, 1982; Gabrielse, 1985; Jarrard, 1986; Umhoefer, 1987; Oldow et al., 1990).

The Leeward Antilles (Aruba, Bonaire and Curacao, Fig. 1) include a series of juxtaposed Upper Cretaceous intra-oceanic volcanic arc and plateau remnants covered by several turbidite-like sedimentary units, Paleogene conglomerates and carbonates (Beets et al., 1977; Thompson et al., 2004; Van der Lelij et al., 2010; Wright and Wyld, 2010, Fig. 1). This oceanic domain experienced several Late Cretaceous to Late Paleogene tectonic events, including intra-oceanic arc-plateau juxtaposition, collision with the continental margin of northern South America and overimposed oblique convergence associated to post-Middle Eocene extensional events, of N–S and SW–NE extension that caused the lateral segmentation of a former continuous Caribbean orogen as a consequence of the oblique subduction of the Caribbean plate under the South American continent (Macellari, 1995; Beardsley and Ave-Lallemant, 2007; Gorney et al., 2007; Van der Lelij et al., 2010; Wright and Wyld, 2010; Xie et al., 2010).

The post-Eocene tectonic evolution of the Leeward Antilles (Gorney et al., 2007) and adjacent basins in northern Colombia and northwestern Venezuela such as the Lower Magdalena, Lower and

*. Corresponding author. Tel.: +57 4 3147953543.
*E-mail address:* szapatah@gmail.com (S. Zapata).

http://dx.doi.org/10.1016/j.jsames.2014.02.009
0895-9811/

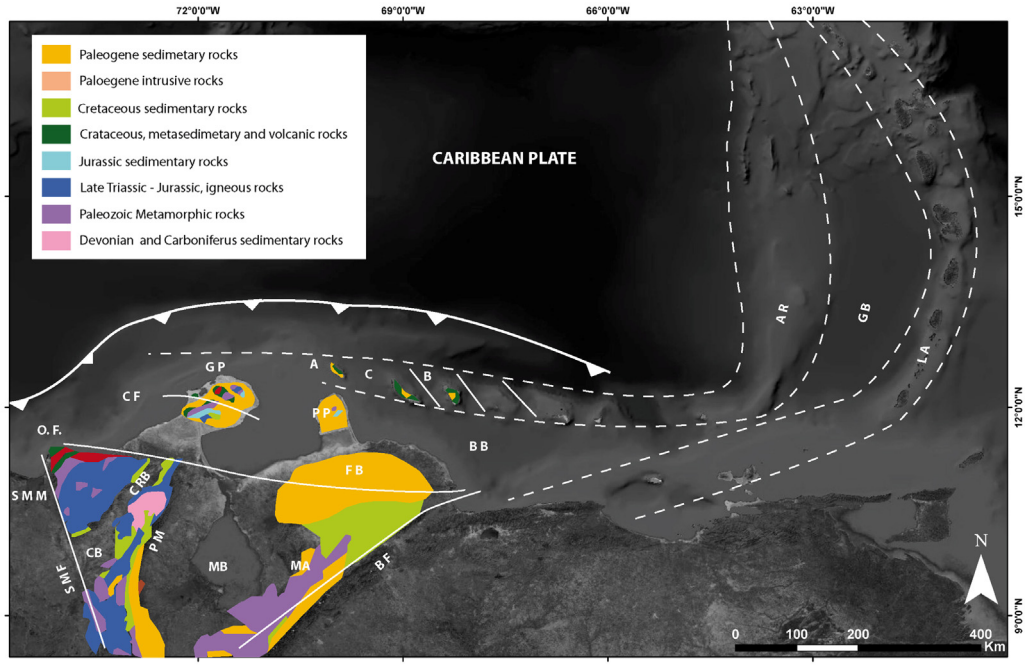


**Fig. 1.** Tectonic setting and basement units of southeastern Caribbean modified from Gorney et al. (2007) and Ayala et al. (2012), over satellite i-cube image. The different tectonic blocks and structures are labeled: A = Aruba; AR = Aves ridge; B = Bonaire; BB = Bonaire Basin; BF = Bocono Fault; C = Curacao; CF = Cuisa Fault; CB = Catatumbo Basin; CRB = Cesar-Rancheria Basin; FB = Falcón Basin; GB = Grenada Basin; GP = Guajira Peninsula; LA = Lesser Antilles; SMF = Santa Marta Fault; SMM = Santa Marta Massif; MA = Mérida Andes; MB = Maracaibo Basin; OF = Oca Fault; PP = Paraguaná Peninsula and PM = Perija Massif.

Upper Guajira basins and the Falcon Basin (Fig. 1, Muessig, 1984; Macellari, 1995; Vence, 2008; Montes et al., 2010; Quiroz and Jaramillo, 2010; Zapata et al., 2010) preserves the tectonic record of the oblique convergence.

The presence of stranded Precambrian clasts in conglomerates of the Soebi Blanco Formation in Bonaire (Priem et al., 1986) have been used to suggests that the Leeward Antilles block was dextrally displaced from the northeastern Colombia South American Basement Massifs (SABM) as part of the aforementioned transtensional tectonics.

In this contribution we used integrated provenance techniques (clast counting, zircon U–Th/He thermochronology, sandstone petrography, heavy mineral analysis and U–Pb detrital zircon geochronology) in the Eocene conglomerates and sandstones from the Soebi Blanco Formation which are exposed over the oceanic rocks of Bonaire basement, in order to: (1) review the stratigraphy and used the provenance to test the existence of source areas and provincialism in NE and NW Colombian and Venezuelan basins during the isolation and formation of local topography linked to the extensional tectonic regime (Macellari, 1995; Pindell et al., 1998; Müller et al., 1999; Escalona and Mann, 2010; Gorney et al., 2007; Pindell, 2009) and (2) reviewed the presence of South American sources and kilometric scale dextral lateral displacement (Priem et al., 1986) associated to transtensional tectonics.

### 1.1. Geological setting

The northeastward migration of the Caribbean plate from a southern Pacific position is responsible for the development of several oceanic-continent orogens formed in the South American margin since the Late Cretaceous (Burke et al., 1984; Lugo and Mann, 1995; Kerr et al., 1996; Pindell et al., 1998, 2005; Spikings et al., 2001, 2005; Vallejo et al., 2006; Cardona et al., 2010a,b; Weber et al., 2009, 2010; Villagomez et al., 2011; Xie et al., 2010). The Leeward Antilles have been interpreted as part of a composite Late Cretaceous oceanic arc and plateau terrane that include volcanic and plutonic rocks that limited the front of the allochthonous Caribbean plate as it advance from a southeastern Pacific position (Thompson et al., 2004; Pindell et al., 2005; Van der Lelij et al., 2010; Wright and Wyld, 2010; Beardsley and Ave-Lallemant, 2007; Gorney et al., 2007; Neill et al., 2011).

Due to the continuous advance of this allochthonous oceanic plate and the oblique subduction (Pindell et al., 1998, 2005; Gorney et al., 2007), the former collisional orogen was replaced by a complex series of transpressional and transtensional post-Paleocene segments (Muessig, 1984; Macellari, 1995), where extensive deformation, block displacement, rotation and basin formation took place (Muessig, 1984; Macellari, 1995; Beardsley and Ave-Lallemant, 2007; Gorney et al., 2007; Montes et al., 2010; Zapata et al., 2010).

### 1.2. Geology of the Leeward Antilles

Aruba, Curacao and Bonaire form part of the Leeward Netherland Antilles in the southern Caribbean margin (Fig. 1). Aruba contains a sequence of stratified basalt flows, volcanoclastic deposits and epiclastic strata, interbedded with marine sediments of Turonian age that are intruded by the 90–87 Ma Aruba Batholith formed as part of an oceanic plateau subsequently modified to an intra-oceanic arc system (Beets et al., 1984; Wright and Wyld, 2010; Van der Lelij et al., 2010). Curacao contains mafic lava flows of 88.9 Ma (Sinton et al., 1998) also formed in an oceanic plateau environment, which together with Aruba may have been part of the Caribbean oceanic plateau (Beets, 1972; Beets et al., 1984; Kerr et al., 1996; Sinton et al., 1998; White et al., 1999).

Magmatic rocks from Bonaire differ from the Aruba and Curacao sequences and are grouped in the Washikemba Formation. This unit records an intra-oceanic arc geochemical signature that

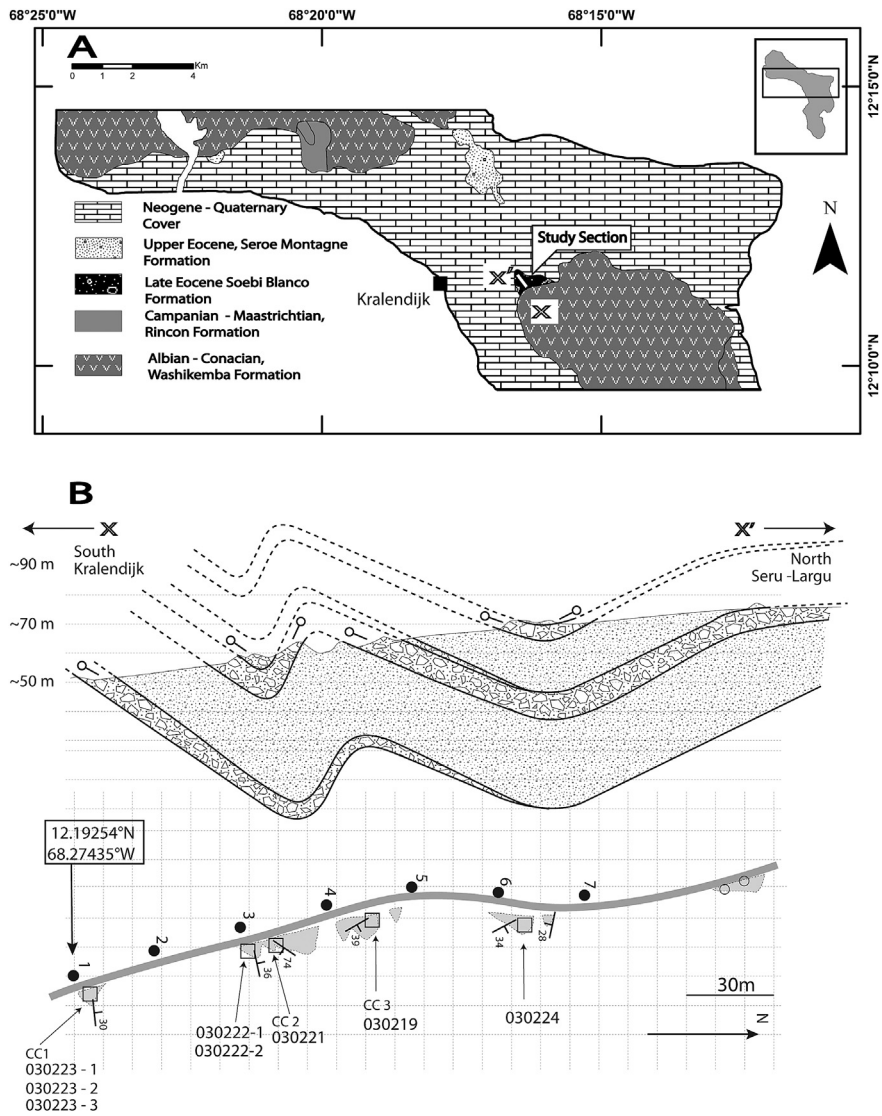


**Fig. 2.** Geology of central Bonaire and sample locations. (A) Simplified geological map of Bonaire after Pijpers (1933) and Beets et al. (1977). (B) Geological cross-section and sampling localities; (CC) = clast counting station.

contrasts with the major oceanic plateau-like signature found in the other two islands. The Washikemba Formation is mainly composed of a sequence of basaltic flows and pyroclastic deposits interbedded with pelagic chert and limestones. All sequences are intruded by basaltic, andesitic and dacitic dikes (Pijpers, 1933; Beets et al., 1977; Wright and Wyld, 2010). These rocks have been related to an intra-oceanic magmatic arc (Klaver, 1976; Beets et al., 1984; Thompson et al., 2004) formed between 100 and 85 Ma (Beets et al., 1977; Priem, 1979; Thompson et al., 2004; Van Der Lelij et al., 2010).

Late Cretaceous Rincón and Middle Curacao turbidites in Bonaire and Curacao with mixed South American and Caribbean provenance covered the oceanic terranes (Beets et al., 1977; Wright and Wyld, 2011).

Paleogene siliciclastic rocks that overlie the older Cretaceous sequences have been reported in Aruba, Curacao and Bonaire. In Bonaire they include conglomerates, sandstones and shales from Soebi Blanco Formation (Beets, 1972; Beets et al., 1977), which are in turn covered by limestones (Beets, 1996; Beets et al., 1977). Whereas in Aruba and Curacao siliciclastic rocks are mainly sandstones which are deposited unconformably over older Cretaceous rocks (Beets, 1972; Wright and Wyld, 2010, Fig. 2A).

The age of the Soebi Blanco Formation is not known in detail. Its age, however, is bracketed by the presence of limestone clasts in the conglomerate that may be derived from the Campanian-Maastrichtian Rincon Formation, and by unconformably overlying limestones of seemingly late Eocene age (Beets et al., 1977).

Since the Late Cretaceous the Leeward Antilles record several tectonic episodes, including ca. 90° clockwise rotation (Hargraves and Shagam, 1969; Stearns et al., 1982), followed by northeast migration and collision with the South American margin (Pindell et al., 1998, 2005; Van Der Lelij et al., 2010).

Structural and thermochronological results have suggest that during the early Eocene Bonaire experienced exhumation and deformation (Beardsley and Ave-Lallemant, 2007; Van Der Lelij et al., 2010), followed by east–west extensional basin formation during the Early Oligocene. Miocene transpression deform the Paleogene sequences in the Leeward Antilles (Beardsley and Ave-Lallemant, 2007; Gorney et al., 2007). Geophysical constraints from the adjacent Leeward Antilles basin also document Late

Eocene-Early Oligocene north–south opening with associated E–W normal faulting followed by overimposed NW faulting (Gorney et al., 2007).

## 2. Methods

### 2.1. Conglomerates and sandstone provenance analysis

Conglomerate clast counting was performed following the ribbon counting method (Howard, 1993). Those clasts <2 cm in size were excluded from the analysis. Results are presented in Table 1. Two sandstones samples interspersed with the conglomerates were collected and point-counted to determine their composition and provenance.

Sandstones petrographic samples were scanned as 1800 dpi high-resolution image and open as a grid with Image J software. This software from the National Institute of Health was used as an automatic sandstone framework counter. Results can be exported and used directly in any graphic or spreadsheet application. Petrographic procedures followed framework analysis after Dickinson (1985) and Folk (1980) and included the identification of various categories of igneous and metamorphic lithics (Table 2).

### 2.2. Heavy minerals

Sandstone samples were crushed, sieved and hydraulically concentrated in the <400 μm fraction. Subsequently sodium polytungstate was used to obtained the >2.89 g/cc fraction. Grains were mounted using the Meltmount® resin with a refraction index of 1.539. Mineral identification of ca. 300 translucent grains was identified following the ribbon method (Mange and Maurer, 1991). Results are presented in Table 3.

### 2.3. U–Pb geochronology

U–Pb LA-ICP-MS zircon geochronology was conducted at the Washington State University at Pullman following procedures established by Chang et al. (2006). Zircon crystals were extracted from samples by traditional methods of crushing and grinding, followed by separation with a Wilfley table, heavy liquids, and a Frantz magnetic separator. Samples were processed such that all zircons were retained in the final heavy mineral fraction. Zircons were incorporated into a 1″ epoxy mount together with standard zircons; the mounts were sanded down to a depth of ~20 microns, polished, and cleaned prior to isotopic analysis. In the case of the zircons recovered from metamorphic rocks, the analyses were done at the zircon rims and cores in order to constrain the late zircon crystallization history (Valencia et al., 2005). In detrital samples, the cores of the grains were analyzed to avoid complex zircon histories (Gehrels et al., 2006).

All LA-ICP-MS U–Pb analyses were conducted at Washington State University using a New Wave Nd: YAG UV 213-nm laser coupled to a Thermo Finnigan Element 2 single collector, double-focusing, magnetic sector ICP-MS. Laser spot size and repetition rate were 30 microns and 10 Hz, respectively. He and Ar carrier gases delivered the sample aerosol to the plasma. Each analysis consisted of a short blank analysis followed by 300 sweeps through masses 204, 206, 207, 208, 232, 235, and 238, taking approximately 35 s.

LA-ICP-MS isotopic analyses are affected by two forms of inter-element fractionation that must be corrected (Kosler and Sylvester, 2003). Uranium–lead data were reduced using Isoplot (Ludwig, 2007). For all samples probability plots were also obtained with the ISOPLOT 3.62 (Ludwig, 2007). Representative age populations were considered when more than three grains overlap in age (Gehrels et al., 2006). This statistical assumption relies on the fact that individual grains may sometimes represent lead-loss trajectories. Analytical results are presented in Tables 4 and 5.

### 2.4. Zircon U–Th/He dating

Measurements of parent and daughter nuclides in zircon grains were performed in Arizona University following the protocol presented in Reiners (2005). To minimize potential zonation effects, grains without obvious inclusions were chosen. Clear, non-magnetic, tetragonal crystals with prism widths of at least 75–100 μm were preferred while grains with prism widths <60 μm were avoided. Morphologies most similar to a tetragonal prism with bipyramidal terminations were selected because alpha-ejection corrections entail the assumption of this characteristic grain morphology (Reiners, 2005; Hourigan et al., 2005). Selected crystals were photographed and their dimensions measured in two perpendicular perspectives parallel to the a1 and a2 crystallographic axes.

Measured dimensions and an assigned morphology were used to calculate the alpha-ejection correction following the Ft correction scheme of Farley (2002). The extraction involved placement of a single crystal into a ~1 mm Nb foil packet that was then slightly closed and placed on a Cu planchet with another in a high vacuum sample chamber connected to the He purification/measurement line. Each foil packet was directly heated using a 10 μm focused laser beam of a 1064-nm Nd-YAG laser to ~1100–1250 °C for 15 min extraction intervals.

All samples were then subjected to at least two re-extractions and He measurements, to assess the extent of degassing of the crystal (typical re-extracts yielded less than 0.3% of previous 4He values). Ratios of 4He/3He were measured for about 10 s following gas release and nominal equilibration time. Measured ratios were corrected for background and interferences on mass 3 (HD+ and H3+), and compared with 4He/3He measured on pipetted aliquots of a manometrically calibrated 4He.

Uranium and Thorium nuclides in degassed zircons were measured by isotope dilution and solution ICP-MS. The approach required spiking with isotopically distinctive U–Th spike, sample-spike equilibration, and dissolution to a final solution suitable for ICP-MS. Zircon dissolution was carried out using HF–$HNO_3$ mixtures which can dissolve the entire Nb foil and zircon content in Parr bombs at temperatures and pressures higher than ambient.

Ratios of 238U/233U and 232Th/229Th were quantified by 2000 measurements of the average intensities in the middle 10% of peak widths in low resolution mode on an Element2 high-resolution ICP-MS. 238U/235U was also measured to check for Pt contamination and mass fractionation. The zircon content in U and Th was calculated from multiple determinations of isotope ratios on pure spike and spiked normal containing 1–4 ng of isotopically normal U and Th. In zircon, He dating alpha-ejection was corrected using the method of Farley et al. (1996) and Farley (2002).

**Table 1**
Results of conglomerate clast counting.

| | Counted Points | Igneous Plutonic rocks | Igneous Volcanic Rocks | Sandstones | Quartzs | Cherts | Gneisses |
|---|---|---|---|---|---|---|---|
| CC1 (%) | 100 | 15.0 | 43.0 | 9.00 | 1.00 | 32.0 | 0.0 |
| CC1 | | 15 | 43 | 9 | 1 | 32 | 0 |
| CC2 (%) | 100 | 21.0 | 45.0 | 3.00 | 4.0 | 25.0 | 2.0 |
| CC2 | | 21 | 45 | 3 | 4 | 25 | 2 |
| CC3 (%) | 84 | 36.9 | 52.4 | 2.38 | 0 | 5.95 | 2.4 |
| CC3 | | 31 | 44 | 2 | 0 | 5 | 2 |

**Table 2**
Sandstone framework analysis. Qm = monocrystalline quartz, Qpd = difuse polycrystalline quartz, Pl = plagioclase, Ls = sedimentary lithic, Lmm = micaceous metamorphic lithic, Lvf = porphyritic lithic, Lvm = mafic volcanic lithic, Lpf = plutonic felsic lithic, Lpm = plutonic mafic lithic, Mosc = muscovite, and Op = opaque.

| Sample | Quartz | | Feldespar | Lithics | | | | | | Accessories | | Modal calculations | | | | | Total lithics | | |
|---|---|---|---|---|---|---|---|---|---|---|---|---|---|---|---|---|---|---|---|
| | Qm | Qpd | Pl | Ls | Lmm | Lvf | Lvm | Lpf | Lpm | Mosc | Opaco | Qt | Qm | F | L | Lt | St | Mt | Vt |
| 030219 (%) | 18.2 | 11.4 | 4.00 | 2 | 11.6 | 7.40 | 36.4 | 0.30 | 3.40 | 3.1 | 2.30 | 31.2 | 19.2 | 4.20 | 64.6 | 64.6 | 3.30 | 19.1 | 77.7 |
| 030219 | 64 | 40 | 14 | 7 | 41 | 26 | 128 | 1 | 12 | 11 | 8 | | | | | | | | |
| 030221 (%) | 17.7 | 12.6 | 2.30 | 0.3 | 14.0 | 4.00 | 24.9 | 3.40 | 11.7 | 3.10 | 6.00 | 33.3 | 19.5 | 2.50 | 64.2 | 64.2 | 0.50 | 24.0 | 75.5 |
| 030221 | 62 | 44 | 8 | 1 | 49 | 14 | 87 | 12 | 41 | 11 | 21 | | | | | | | | |

Propagated errors for zircon He ages based on the analytical uncertainty associated with U, Th, and He measurements are ~4% ($2\sigma$) for laser samples (Reiners, 2005; Farley, 2002). Nevertheless, a 6% ($2\sigma$) uncertainty for all samples is reported based on the reproducibility of replicate analyses of laboratory standard samples (Reiners, 2005). All analytical results are presented in Table 6.

## 3. Results

We analyzed conglomerate and sandstone from the Soebi Blanco Formation which have been interpreted as a fluvial related unit covered by carbonatic rocks (Beets et al., 1977). Due to their grain size and sedimentary environment, the associated conglomerates and sandstones associated provide a robust view of the composition of the most proximal (<100 km) source areas (Ferguson et al., 1996; Kodama, 1994). The Soebi Blanco was described by Beets et al. (1977) as a 400 m thick sequence of fluvial conglomerates, with intercalated sandstones and shales (Fig. 2A).

### 3.1. Field relations and sampling

Sampling was performed in a deformed road-side conglomerate–sandstone sequence that shows asymmetrical folding verging to the south (Fig. 2B). The lower contact is not exposed, while to the top there is a sequence of nearly undeformed, but tilted, reef-forming carbonates (Beets et al., 1977). Conglomerate clast counting was performed in three different localities. Interbedded sandstones were also sampled for petrography, heavy mineral analysis and U–Pb detrital geochronology.

We also selected three gneissic pebbles for U–Pb and U–Th/He zircon analysis to test for the value of previously reported TIMS multigrain analysis (Priem et al., 1986) and characterized the ca. 170 °C segment of the low temperature history of the continental source area that may preserve the history of early Cenozoic tectonic events.

### 3.2. Conglomerates clast counting

Conglomerates are polymictic and matrix-supported, with clast size ranging between 2 cm and 15 cm. Clast shape is predominantly rounded to sub-rounded. Counting results are presented on Table 1. All the three counting stations are characterized by abundant volcanic and plutonic rocks, sedimentary rocks such as chert and minor sandstones, milky quartz and gneissic clasts. We have discriminate six major compositional groups: (1) mafic volcanic rocks with minor intermediate porphyritic rocks (15–36%); (2) mafic plutonic rocks such as diorites and gabbro with minor granites (43–52%); (3) marine sedimentary rocks including chert and algae limestones (6–32%); (4) rounded milky quartz and quartzites (0–4%); (5) medium grain coarse quartz-sandstones and lithic-sandstones (2–9%); and (6), micaceous gneissic clasts (0–2%). Gneissic metamorphic pebbles were found in two of the counting localities (Fig. 3A).

### 3.3. Sandstone petrography and heavy mineral analysis

The sandstones associated to the Soebi Blanco Formation conglomerates are medium to coarse grained, with rounded to subrounded grains and poor sorting. Compositionally the sandstones are lithoarenites (Fig. 4A). Lithics include abundant mafic volcanics, porphyritic, micaceous metamorphic, gneissic, monocrystalline quartz, opaque minerals and muscovite (Table 2). Within the Dickinson (1985) discrimination diagram, they plot the recycled orogen field as expected from the erosion of multiple source areas (Fig. 4B).

Heavy minerals include abundant mafic and unstable minerals such as epidote, olivine and pyroxenes with minor amphibole and lower contents of more stable to ultra-stable, zircon, apatite, garnet, rutile and muscovite (Fig. 3B).

### 3.4. U–Pb zircon geochronology of metamorphic clasts

Three gneissic pebbles were analyzed. Zircons from sample 030222-1 are rounded to sub-rounded, with 1:2 to 1:4 width/length ratios and grain sizes between 300 and 1000 μm. Cathodoluminescence images show oscillatory-zoned textures and bright homogenous zircons and the presence of old reabsorbed cores with interrupted zoning patterns indicative of successive metamorphic and associated melting events. U–Pb geochronological results from 31 grains yield ages between 1150 and 1250 Ma. The oldest cores include ages of 1239 ± 13 Ma and 1371 ± 15 Ma and together with the zircon age variation suggest a paragneissic origin. Younger age of 876.6 ± 13 Ma in homogenous zircons may be related to an overprinting metamorphic event (Fig. 5A). Sample 030223-2 includes sub-rounded to angular zircons with 1:3 to 1:4 width/length ratios and crystal sizes that range between 100 and 300 μm. Cathodoluminescence images show complex internal textures with oscillatory cores surrounded by bright rims related to metamorphic and melt-related growth events (Fig. 5B). U–Pb geochronological results from 59 grains yield ages between 1000 and 1250 Ma. The oldest oscillatory zoning cores have ages that span between 1483.5 ± 13.2 Ma and 1342 ± 9.8 Ma. Some metamorphic rims record the youngest ages of 694.3 ± 13 Ma and 886.7 ± 45.3 Ma (Fig. 5B) that we relate to a lead-loss event of uncertain age. Finally, zircons from sample 030223-3 are also subrounded to angular with 1:2 to 1:4 width/length ratios and a size that varies between 100 and 500 μm. Cathodoluminescence images show complex oscillatory cores with interrupted zoning patterns, occasionally bounded by thin metamorphic rims. Results from 40 grains yield a main population age of 1000–1250 Ma. The oldest cores have ages between of 1494.8 Ma and 1375.4 Ma. Similar younger ages of 746.4 ± 12.1 Ma and 842.8 ± 16.4 Ma are also common (Fig. 5C).

### 3.5. Sandstone U–Pb detrital zircon geochronology

We analyzed one sandstone sample (030223-1) from the matrix in the Eocene Soebi Blanco conglomerate (Fig. 6). The analytical

**Table 3**
Results from Heavy minerals analyses.

| Sample | Counted Points | Epidote | Ortopiroxene | Olivine | Clinopiroxene | Clinozoicite | Zoicite | Anphibole | Garnet | Zircon | Rutile | Apatite | Moscovite |
|---|---|---|---|---|---|---|---|---|---|---|---|---|---|
| 030224 (%) | 350 | 34.9 | 22.3 | 6.57 | 19.1 | 2.00 | 6.29 | 5.14 | 1.14 | 0.571 | 0.857 | 0.57 | 0.57 |
| 030224 | | 122 | 78 | 23 | 67 | 7 | 22 | 18 | 4 | 2 | 3 | 2 | 2 |
| 030222-2 (%) | 356 | 42.1 | 9.8 | 11.0 | 23.6 | 1.12 | 2.81 | 2.25 | 1.69 | 1.40 | 2.25 | 0.843 | 1.12 |
| 030222-2 | | 150 | 35 | 39 | 84 | 4 | 10 | 8 | 6 | 5 | 8 | 3 | 4 |

results are presented in Table 5. The 100 analyzed zircon crystals are sub-angular in shape. Cathodoluminescence images show homogenous metamorphic textures and some oscillatory igneous grains. Three major age populations can be identified: a Mesoproterozoic to early Paleozoic peaks of 1000–1200 Ma, 750–950 Ma and 500–750 Ma. The other Phanerozoic age populations are represented by a Permo-Triassic peak (250 Ma). Older Paleoproterozoic ages are also common but less prominent, and a young single Cretaceous zircon of 70.1 Ma was also found. However the statistical and geological meaning of this age, as part of an age population or a lead-loss event is not possible to resolve (Gehrels et al., 2006).

### 3.6. (U–Th/He), thermochronology

We analyzed nine zircons from three gneissic clasts of the Soebi Blanco Formation conglomerates. Sample 030223-3 yields two consistent ages of 57.5 and 61.9 Ma. Sample 031222-1 records the youngest ages (50–54 Ma, Table 6). An older age of 306.5 Ma was also found in this sample, are probably related to micro-inclusions which commonly yield older ages in zircons (Fitzgerald, 2006). Paleocene ages of 63–65 Ma were obtained in three analyzed zircons from sample 030223-2.

### 3.7. Provenance and age of the Soebi Blanco Formation

Previous workers have bracketed the age of Soebi Blanco Formation by the presence of pebbles from the Upper Cretaceous Rincón Formation and by the overlying upper Eocene limestones (Beets et al., 1977). We present new age constrain by considering the U–Th/He ages obtained in the three Precambrian gneissic clasts.

The U–Th/He ages are interpreted here as detrital cooling ages and a major vestige of a Paleogene cooling event within the source area. We make this assumption based on low thickness (<1 km) reported for the Oligocene and Miocene sequences, which is overlying the Soebi Blanco Fm. conglomerates in Bonaire and the adjacent offshore regions (Beets et al., 1977; Fouke et al., 1996; Gorney et al., 2007). Also, the lack of post-Eocene magmatism in the region precludes the ca. 170 °C thermal resetting of the U–Th/He system in zircon (Reiners, 2005). Thus, the new U–Th/He detrital zircon ages from the gneissic clasts (as young as 50.1 Ma), constrain the deposition and deformation of this formation to be post-middle Eocene (<50 Ma) and pre-Late Eocene.

The new provenance analysis from conglomerates and sandstones of the Soebi Blanco formation suggests the existence of at least three main proximal source areas: (1) a magmatic domain composed of abundant mafic volcanic rocks, granitites and porphyritic dikes; (2) marine sedimentary rocks; and (3) quartzose and gneissic metamorphic source area.

Whereas the former two source areas can be found in the basement of the Leeward Antilles and Caribbean-related magmatic rocks (Beets et al., 1977; Thompson et al., 2004; Wright and Wyld, 2010), the metamorphic components, including gneissic and schists clasts with heavy minerals such as garnet, rutile and muscovite, can only have their counterpart in a more quartzose and sialic continental basement. A source area with the sialic components above described can be found along the SABM, a margin characterized by >150 Ma and zircon ages (Cordani et al., 2005; Cardona et al., 2006; Weber et al., 2010) similar to those found in the analyzed sandstones and conglomerate gneissic clasts (Fig. 6A). The new U–Pb single grain analyses confirm the previous Precambrian ages obtained in zircon by the U–Pb conventional multigrain analysis of the gneissic clasts presented by Priem et al. (1986), and clearly establish the presence of Precambrian proximal sources. However, they also show that the Precambrian zircon forming record is far more complex than obtained by Priem et al. (1986).

The absence of proximal Precambrian gneissic sources in the Leeward Antilles or the adjacent Paraguaná Peninsula and Falcon Basin in Venezuela was used by Priem et al. (1986) to suggest that this formation and the Bonaire oceanic block was in a position proximal to the Guajira Peninsula of northern Colombia during the Eocene where Grenvillian basement of 1000–1200 Ma has been firmly established (Cordani et al., 2005). The new Jurassic, Permo-Triassic and Greenville age population from the Soebi Blanco conglomerate matrix are also characteristic of the SABM (Tschanz et al., 1974; Lockwood, 1965; Cordani et al., 2005; Cardona et al., 2010b; Weber et al., 2010). However, recently published geochronological data from the Paraguana Peninsula and offshore Falcon region have revealed the existence of the same Permian–Triassic and Precambrian gneissic and plutonic rocks similar to those found in the Guajira region (Grande and Urbani, 2009; Mendi et al., 2013).

Thus, all blocks from SABM are still possible sources for the gneissic clasts of the Soebi Blanco Formation in Bonaire. Discriminating among them may be achieved when a more complete geochronological/thermochronological database exists. The choice of basement massif as the source impacts the magnitude of the relative tectonic translation of the Leeward Antilles from the northern South America continental margin. Those blocks share similar basements, compose by metamorphic Grenvillian rocks intruded by Jurassic igneous rocks and with deformed Jurassic–Cretaceous marine sediments (Macdonald, 1964; Tschanz et al., 1974; Lockwood, 1965; Gonzalez de Juana et al., 1980; Cordani et al., 2005; Grande and Urbani, 2009; Mendi et al., 2013) suggesting that they were probably amalgamated in the Late Cretaceous in a close position to the Leeward Antilles.

If the choice remains the Guajira Peninsula as suggested by Priem et al. (1986), 300 km of right-lateral displacement are needed. At least 200 km of relative dextral displacement regarding Paraguana Peninsula which is the closest block, while a larger 350–400 km displacement would be needed considering the farthest block witch is Santa Marta massif.

The older 65–50 Ma U–Th/He zircon thermochronological results found in the Soebi Blanco Formation Precambrian gneissic clasts are similar to the fast cooling ages recognized in oceanic and continental crystalline basement rocks from the Leeward Antilles (Van der Lelij et al., 2010) and the northern Margin of Colombia, including the Guajira and Santa Marta regions (Cardona et al., 2011a; Villagomez et al., 2011) and Venezuela (Sisson, 2008), supporting the lateral correlation between basins and uplift regions.

**Table 4**
U–Pb LA-ICP-MS analytical and age results from the analyzed metamorphic clasts.

| Sample name | 238U 206Pb | 1 Sigma % error | 207 Pb 206 Pb | 1 Sigma % error | 206/238 age | 1 Sigma abs err | 207/206 age | 1 Sigma abs err | Best age | 1 Sigma abs err |
|---|---|---|---|---|---|---|---|---|---|---|
| 030222-1_31 | 5.271 | 0.020 | 0.07510 | 0.0073 | 1120 | 20.6 | 1071 | 15 | 1071 | 15 |
| 030222-1_30 | 5.524 | 0.020 | 0.08020 | 0.0060 | 1073 | 19.9 | 1201 | 12 | 1201 | 12 |
| 030222-1_29 | 5.150 | 0.020 | 0.07960 | 0.0048 | 1144 | 20.9 | 1187 | 9 | 1187 | 9.4 |
| 030222-1_28 | 5.273 | 0.020 | 0.07850 | 0.0066 | 1120 | 20.9 | 1158 | 13 | 1158 | 13 |
| 030222-1_27 | 5.6756 | 0.021 | 0.08090 | 0.0049 | 1046 | 20.2 | 1220 | 10 | 1220 | 10 |
| 030222-1_26 | 5.248 | 0.025 | 0.07960 | 0.0093 | 1124 | 25.9 | 1186 | 18 | 1186 | 18 |
| 030222-1_25 | 5.213 | 0.021 | 0.07930 | 0.0062 | 1131 | 21.8 | 1180 | 12 | 1180 | 12 |
| 030222-1_24 | 5.212 | 0.023 | 0.08060 | 0.0072 | 1132 | 24.3 | 1213 | 14 | 1213 | 14 |
| 030222-1_23 | 5.214 | 0.021 | 0.08030 | 0.0052 | 1131 | 21.6 | 1204 | 10 | 1204 | 10 |
| 030222-1_22 | 4.711 | 0.020 | 0.08120 | 0.0071 | 1241 | 22.4 | 1225 | 14 | 1225 | 14 |
| 030222-1_21 | 6.678 | 0.025 | 0.07810 | 0.0055 | 900 | 21.2 | 1149 | 11 | 1149 | 11 |
| 030222-1_20 | 4.762 | 0.019 | 0.08040 | 0.0088 | 1229 | 21.7 | 1207 | 17 | 1207 | 17 |
| 030222-1_19 | 6.865 | 0.017 | 0.07090 | 0.0035 | 877 | 13.5 | 954 | 7 | 877 | 13 |
| 030222-1_18 | 4.751 | 0.020 | 0.08180 | 0.0067 | 1231 | 22.5 | 1240 | 13 | 1240 | 13 |
| 030222-1_17 | 5.263 | 0.016 | 0.07950 | 0.0045 | 1121 | 16.6 | 1185 | 9 | 1185 | 8.9 |
| 030222-1_16 | 5.290 | 0.016 | 0.08030 | 0.0048 | 1116 | 16.2 | 1205 | 10 | 1205 | 10 |
| 030222-1_15 | 5.4155 | 0.019 | 0.07920 | 0.0077 | 1092 | 19.3 | 1177 | 15 | 1177 | 15 |
| 030222-1_14 | 5.127 | 0.018 | 0.08000 | 0.0062 | 1149 | 18.4 | 1197 | 12 | 1197 | 12 |
| 030222-1_13 | 6.790 | 0.055 | 0.07630 | 0.0064 | 886 | 45.3 | 1104 | 13 | 886 | 45 |
| 030222-1_12 | 4.955 | 0.017 | 0.07900 | 0.0068 | 1185 | 18.7 | 1173 | 13 | 1185 | 19 |
| 030222-1_11 | 5.403 | 0.017 | 0.08010 | 0.0048 | 1095 | 16.7 | 1199 | 10 | 1199 | 9.5 |
| 030222-1_10 | 5.206 | 0.017 | 0.07910 | 0.0071 | 1133 | 17.6 | 1176 | 14 | 1176 | 14 |
| 030222-1_9 | 6.702 | 0.041 | 0.08750 | 0.0079 | 897 | 34.1 | 1371 | 15 | 1371 | 15 |
| 030222-1_8 | 5.204 | 0.018 | 0.07950 | 0.0079 | 1133 | 19.1 | 1186 | 16 | 1186 | 15 |
| 030222-1_7 | 5.403 | 0.016 | 0.07850 | 0.0041 | 1095 | 15.6 | 1160 | 8 | 1160 | 8.2 |
| 030222-1_6 | 5.446 | 0.016 | 0.08070 | 0.0058 | 1087 | 16.3 | 1213 | 11 | 1213 | 11 |
| 030222-1_5 | 5.087 | 0.017 | 0.07860 | 0.0068 | 1157 | 18.4 | 1162 | 13 | 1162 | 13 |
| 030222_1_4 | 5.976 | 0.016 | 0.07645 | 0.0054 | 997 | 14.4 | 1107 | 11 | 1107 | 11 |
| 030222-1_3 | 5.259 | 0.015 | 0.07960 | 0.0033 | 1122 | 14.9 | 1186 | 7 | 1186 | 6.5 |
| 030222-1_2 | 5.326 | 0.015 | 0.07880 | 0.0049 | 1109 | 15.7 | 1167 | 10 | 1167 | 10 |
| 030222-1_1 | 5.167 | 0.016 | 0.07970 | 0.0046 | 1141 | 16.6 | 1188 | 9 | 1188 | 9.1 |
| 030223-2_59 | 5.070 | 0.061 | 0.07790 | 0.0047 | 1161 | 64.7 | 1146 | 9 | 1146 | 9.3 |
| 030223-2_58 | 5.244 | 0.062 | 0.08390 | 0.0045 | 1125 | 63.2 | 1291 | 9 | 1291 | 8.6 |
| 030223-2_57 | 5.446 | 0.062 | 0.07680 | 0.0058 | 1087 | 61.2 | 1115 | 12 | 1115 | 11.5 |
| 030223-2_56 | 5.156 | 0.061 | 0.07890 | 0.0048 | 1143 | 63.8 | 1169 | 10 | 1169 | 9.5 |
| 030223-2_55 | 5.047 | 0.062 | 0.07980 | 0.0050 | 1165 | 65.2 | 1192 | 10 | 1192 | 9.8 |
| 030223-2_54 | 5.681 | 0.062 | 0.07420 | 0.0046 | 1045 | 59 | 1047 | 9 | 1047 | 9.2 |
| 030223-2_53 | 4.928 | 0.062 | 0.07740 | 0.0046 | 1191 | 66.8 | 1130 | 9 | 1130 | 9.1 |
| 030223-2_52 | 5.804 | 0.062 | 0.08030 | 0.0058 | 1025 | 58.6 | 1205 | 11 | 1205 | 11.4 |
| 030223-2_51 | 4.763 | 0.077 | 0.07760 | 0.0088 | 1229 | 85.2 | 1138 | 17 | 1138 | 17.3 |
| 030223-2_50 | 5.543 | 0.071 | 0.07170 | 0.0066 | 1069 | 69.9 | 978 | 13 | 978 | 13.3 |
| 030223-2_49 | 7.016 | 0.063 | 0.07380 | 0.0080 | 859 | 50.8 | 1035 | 16 | 859 | 50.8 |
| 030223-2_48 | 6.902 | 0.084 | 0.07820 | 0.0070 | 872 | 67.7 | 1153 | 14 | 1153 | 13.8 |
| 030223-2_47 | 6.018 | 0.062 | 0.07580 | 0.0050 | 991 | 56.2 | 1089 | 10 | 1089 | 9.9 |
| 030223-2_46 | 5.218 | 0.062 | 0.08000 | 0.0050 | 1130 | 63.6 | 1196 | 10 | 1196 | 9.8 |
| 030223-2_45 | 4.864 | 0.061 | 0.08080 | 0.0046 | 1205 | 66.9 | 1217 | 9 | 1217 | 9.0 |
| 030223-2_44 | 4.192 | 0.062 | 0.08620 | 0.0051 | 1379 | 76 | 1342 | 10 | 1342 | 9.8 |
| 030223-2_43 | 5.394 | 0.062 | 0.07530 | 0.0069 | 1096 | 61.9 | 1077 | 14 | 1096 | 62 |
| 030223-2_42 | 6.205 | 0.063 | 0.07350 | 0.0044 | 963 | 55.8 | 1028 | 9 | 963 | 56 |
| 030223-2_41 | 5.978 | 0.062 | 0.07730 | 0.0076 | 997 | 56.7 | 1130 | 15 | 1130 | 15 |
| 030223-2_40 | 5.562 | 0.076 | 0.07530 | 0.0112 | 1066 | 74.1 | 1075 | 22 | 1075 | 22 |
| 030223-2_39 | 5.821 | 0.076 | 0.07450 | 0.0068 | 1022 | 71 | 1055 | 14 | 1055 | 14 |
| 030223-2_38 | 5.433 | 0.075 | 0.07630 | 0.0081 | 1089 | 74.9 | 1104 | 16 | 1104 | 16 |
| 030223-2_37 | 4.263 | 0.075 | 0.09280 | 0.0070 | 1358 | 91.2 | 1484 | 13 | 1484 | 13 |
| 030223-2_36 | 5.518 | 0.075 | 0.07460 | 0.0092 | 1074 | 74.2 | 1059 | 19 | 1059 | 19 |
| 030223-2_35 | 4.938 | 0.075 | 0.08170 | 0.0072 | 1189 | 80.9 | 1239 | 14 | 1239 | 14 |
| 030223-2_34 | 5.963 | 0.076 | 0.07790 | 0.0089 | 999 | 69.5 | 1144 | 18 | 1144 | 18 |
| 030223-2_33 | 5.006 | 0.075 | 0.07680 | 0.0070 | 1174 | 80.1 | 1116 | 14 | 1116 | 14 |
| 030223-2_32 | 4.772 | 0.075 | 0.07930 | 0.0067 | 1226 | 83.6 | 1179 | 13 | 1179 | 13 |
| 030223-2_31 | 5.399 | 0.075 | 0.07700 | 0.0075 | 1095 | 75.3 | 1121 | 15 | 1121 | 15 |
| 030223-2_30 | 5.070 | 0.075 | 0.08230 | 0.0070 | 1161 | 79.4 | 1253 | 14 | 1253 | 14 |
| 030223-2_29 | 5.154 | 0.075 | 0.07650 | 0.0080 | 1143 | 78.4 | 1107 | 16 | 1107 | 16 |
| 030223-2_28 | 4.558 | 0.076 | 0.07830 | 0.0090 | 1279 | 88 | 1154 | 18 | 1154 | 18 |
| 030223-2_27 | 5.029 | 0.076 | 0.07720 | 0.0086 | 1169 | 80.2 | 1127 | 17 | 1127 | 17 |
| 030223-2_26 | 5.159 | 0.075 | 0.07990 | 0.0071 | 1142 | 78.3 | 1194 | 14 | 1194 | 14 |
| 030223-2_25 | 8.794 | 0.083 | 0.07120 | 0.0124 | 694 | 54.1 | 965 | 25 | 694 | 54 |
| 030223-2_24 | 6.314 | 0.078 | 0.07720 | 0.0071 | 948 | 68.1 | 1126 | 14 | 1126 | 14 |
| 030223-2_23 | 5.290 | 0.075 | 0.07910 | 0.0068 | 1116 | 76.6 | 1175 | 13 | 1175 | 13 |
| 030223-2_22 | 5.122 | 0.075 | 0.08270 | 0.0075 | 1150 | 78.8 | 1263 | 15 | 1263 | 15 |
| 030223-2_21 | 6.726 | 0.075 | 0.07600 | 0.0093 | 894 | 62.6 | 1095 | 19 | 894 | 63 |
| 030223-2_20 | 5.076 | 0.059 | 0.07890 | 0.0062 | 1159 | 61.9 | 1169 | 12 | 1169 | 12 |
| 030223-2_19 | 5.057 | 0.059 | 0.07820 | 0.0062 | 1163 | 62.3 | 1152 | 12 | 1152 | 12 |
| 030223-2_18 | 5.101 | 0.059 | 0.08030 | 0.0065 | 1154 | 61.8 | 1203 | 13 | 1203 | 13 |

(*continued on next page*)

**Table 4** (*continued*)

| Sample name | 238U 206Pb | 1 Sigma % error | 207 Pb 206 Pb | 1 Sigma % error | 206/238 age | 1 Sigma abs err | 207/206 age | 1 Sigma abs err | Best age | 1 Sigma abs err |
|---|---|---|---|---|---|---|---|---|---|---|
| 030223-2_17 | 4.706 | 0.059 | 0.08760 | 0.0066 | 1242 | 66.1 | 1373 | 13 | 1242 | 66 |
| 030223-2_16 | 4.428 | 0.059 | 0.08450 | 0.0076 | 1313 | 69.2 | 1304 | 15 | 1304 | 15 |
| 030223-2_15 | 4.881 | 0.058 | 0.08450 | 0.0060 | 1202 | 63.6 | 1304 | 12 | 1304 | 12 |
| 030223-2_14 | 6.215 | 0.063 | 0.07550 | 0.0099 | 962 | 56.4 | 1081 | 20 | 1081 | 20 |
| 030223-2_13 | 6.523 | 0.058 | 0.07150 | 0.0066 | 920 | 49.9 | 972 | 13 | 920 | 50 |
| 030223-2_12 | 5.583 | 0.059 | 0.07620 | 0.0078 | 1062 | 57.4 | 1100 | 15 | 1100 | 15 |
| 030223-2_11 | 4.773 | 0.058 | 0.08330 | 0.0070 | 1226 | 64.9 | 1276 | 14 | 1276 | 14 |
| 030223-2_10 | 5.720 | 0.058 | 0.07760 | 0.0060 | 1039 | 55.6 | 1138 | 12 | 1138 | 12 |
| 030223-2_9 | 6.780 | 0.060 | 0.07560 | 0.0081 | 887 | 49.1 | 1084 | 16 | 887 | 49 |
| 030223-2_8 | 4.032 | 0.058 | 0.08370 | 0.0073 | 1428 | 74.4 | 1285 | 14 | 1285 | 14 |
| 030223-2_7 | 5.157 | 0.059 | 0.07980 | 0.0068 | 1143 | 61.3 | 1193 | 13 | 1193 | 13 |
| 030223-2_6 | 5.278 | 0.058 | 0.07830 | 0.0065 | 1119 | 59.5 | 1155 | 13 | 1155 | 13 |
| 030223-2_5 | 5.137 | 0.058 | 0.07870 | 0.0063 | 1147 | 60.9 | 1165 | 13 | 1165 | 13 |
| 030223-2_4 | 5.517 | 0.058 | 0.07770 | 0.0071 | 1074 | 57.5 | 1138 | 14 | 1138 | 14 |
| 030223-2_3 | 4.450 | 0.059 | 0.08270 | 0.0074 | 1307 | 69.3 | 1262 | 14 | 1262 | 14 |
| 030223-2_2 | 6.508 | 0.060 | 0.06960 | 0.0114 | 922 | 51 | 917 | 23 | 922 | 51 |
| 030223-2_1 | 5.020 | 0.058 | 0.08560 | 0.0085 | 1171 | 62.1 | 1330 | 16 | 1330 | 16 |
| 030223-3_40 | 6.151 | 0.015 | 0.07500 | 0.0055 | 971 | 13 | 1069 | 11 | 1069 | 11 |
| 030223-3_39 | 5.624 | 0.015 | 0.07760 | 0.0057 | 1055 | 14.5 | 1136 | 11 | 1136 | 11 |
| 030223-3_38 | 5.821 | 0.014 | 0.07730 | 0.0054 | 1022 | 13.5 | 1129 | 11 | 1129 | 11 |
| 030223-3_37 | 5.488 | 0.014 | 0.07670 | 0.0052 | 1079 | 14 | 1114 | 10 | 1114 | 10 |
| 030223-3_36 | 6.042 | 0.016 | 0.07700 | 0.0054 | 987 | 14.7 | 1121 | 11 | 1121 | 11 |
| 030223-3_35 | 5.663 | 0.016 | 0.07550 | 0.0060 | 1048 | 15.8 | 1081 | 12 | 1081 | 12 |
| 030223-3_34 | 5.879 | 0.018 | 0.07580 | 0.0058 | 1013 | 16.7 | 1090 | 12 | 1090 | 12 |
| 030223-3_33 | 5.848 | 0.019 | 0.07470 | 0.0056 | 1018 | 17.6 | 1060 | 11 | 1060 | 11 |
| 030223-3_32 | 5.243 | 0.021 | 0.08050 | 0.0065 | 1125 | 21.4 | 1210 | 13 | 1210 | 13 |
| 030223-3_31 | 5.397 | 0.020 | 0.07940 | 0.0060 | 1096 | 20.1 | 1182 | 12 | 1182 | 12 |
| 030223-3_30 | 7.160 | 0.021 | 0.07100 | 0.0066 | 843 | 16.4 | 958 | 13 | 843 | 16 |
| 030223-3_29 | 5.625 | 0.019 | 0.07700 | 0.0061 | 1055 | 18.3 | 1121 | 12 | 1121 | 12 |
| 030223-3_28 | 6.782 | 0.021 | 0.07270 | 0.0068 | 887 | 17.7 | 1005 | 14 | 887 | 18 |
| 030223-3_27 | 6.415 | 0.020 | 0.07550 | 0.0080 | 934 | 17.4 | 1081 | 16 | 1081 | 16 |
| 030223-3_26 | 6.113 | 0.018 | 0.07620 | 0.0079 | 977 | 16.5 | 1101 | 16 | 1101 | 16 |
| 030223-3_25 | 6.734 | 0.022 | 0.07090 | 0.0066 | 893 | 18.3 | 956 | 14 | 893 | 18 |
| 030223-3_24 | 5.476 | 0.018 | 0.08070 | 0.0055 | 1081 | 18.2 | 1214 | 11 | 1214 | 11 |
| 030223-3_23 | 6.986 | 0.018 | 0.06990 | 0.0071 | 862 | 14.3 | 924 | 15 | 862 | 14 |
| 030223-3_22 | 6.210 | 0.019 | 0.07450 | 0.0057 | 963 | 16.5 | 1055 | 11 | 1055 | 11 |
| 030223-3_21 | 6.127 | 0.016 | 0.07510 | 0.0060 | 975 | 14.7 | 1072 | 12 | 1072 | 12 |
| 030223-3_20 | 6.671 | 0.020 | 0.07190 | 0.0067 | 901 | 16.7 | 982 | 14 | 901 | 17 |
| 030223-3_19 | 5.770 | 0.016 | 0.07740 | 0.0064 | 1030 | 15.4 | 1132 | 13 | 1132 | 13 |
| 030223-3_18 | 5.767 | 0.017 | 0.07670 | 0.0063 | 1031 | 16 | 1114 | 13 | 1114 | 13 |
| 030223-3_17 | 8.146 | 0.017 | 0.07220 | 0.0066 | 746 | 12.1 | 991 | 13 | 746 | 12 |
| 030223-3_16 | 5.843 | 0.016 | 0.07870 | 0.0066 | 1018 | 15.2 | 1164 | 13 | 1018 | 15 |
| 030223-3_15 | 5.643 | 0.014 | 0.07610 | 0.0063 | 1052 | 13.8 | 1098 | 13 | 1098 | 13 |
| 030223-3_14 | 5.549 | 0.015 | 0.07860 | 0.0063 | 1068 | 14.3 | 1161 | 12 | 1161 | 12 |
| 030223-3_13 | 6.642 | 0.015 | 0.07150 | 0.0067 | 904 | 12.7 | 971 | 14 | 904 | 13 |
| 030223-3_12 | 6.040 | 0.016 | 0.08770 | 0.0075 | 988 | 14.5 | 1375 | 14 | 1375 | 14 |
| 030223-3_11 | 4.542 | 0.020 | 0.09330 | 0.0077 | 1283 | 22.6 | 1495 | 15 | 1495 | 14 |
| 030223-3_10 | 5.267 | 0.020 | 0.07990 | 0.0066 | 1121 | 20.1 | 1196 | 13 | 1196 | 13 |
| 030223-3_9 | 5.663 | 0.015 | 0.07570 | 0.0066 | 1048 | 14.9 | 1088 | 13 | 1088 | 13 |
| 030223-3_8 | 5.907 | 0.030 | 0.07550 | 0.0065 | 1008 | 28.1 | 1082 | 13 | 1082 | 13 |
| 030223-3_7 | 7.118 | 0.019 | 0.07080 | 0.0068 | 848 | 15.4 | 952 | 14 | 848 | 15 |
| 030223-3_6 | 6.204 | 0.036 | 0.07580 | 0.0073 | 963 | 31.7 | 1091 | 15 | 1091 | 15 |
| 030223-3_5 | 6.199 | 0.027 | 0.07780 | 0.0064 | 964 | 23.8 | 1142 | 13 | 1142 | 13 |
| 030223-3_4 | 6.074 | 0.032 | 0.07510 | 0.0070 | 983 | 29.1 | 1072 | 14 | 1072 | 14 |
| 030223-3_3 | 5.213 | 0.024 | 0.07970 | 0.0066 | 1131 | 25 | 1189 | 13 | 1189 | 13 |
| 030223-3_2 | 6.962 | 0.023 | 0.07240 | 0.0067 | 865 | 18.5 | 997 | 14 | 865 | 18 |
| 030223-3_1 | 5.344 | 0.016 | 0.07970 | 0.0072 | 1106 | 16.6 | 1191 | 14 | 1191 | 14 |

### 3.8. Cenozoic Caribbean–South America tectonic interactions

Plate tectonic reconstructions of the Caribbean–South American interactions have suggest that between the Late Cretaceous and the Early Cenozoic, the front of the Caribbean plate was colliding with the South American margin. Leaving behind several arc and plateau remnants and forming orogenic belts that become younger to the northeast as the front of the allochtonous Caribbean plate achieves its Atlantic position (Burke et al., 1984; Lugo and Mann, 1995; Pindell et al., 1998, 2005).

The presence of pre-Mesozoic zircons in the Late Cretaceous turbidite strata of the Knip Group covering the Cretaceous intra-oceanic rocks from Curacao island suggest that the Leeward Antilles which were part of the Caribbean plate were already in close proximity to the SABM (Wright and Wyld, 2010).

In Northern Colombia Guajira and Santa Marta regions the arc-continent collision Caribbean plate with the South American continent is temporally restricted between ca. 70 and 65 Ma (Cardona et al., 2009, 2011, 2013), whereas co-relatable 70–60 Ma tectonic assisted exhumation associated to the same collisional event has been documented in the Leeward Antilles (Van der Lelij et al., 2010).

Provenance results from the Late Cretaceous (Wright and Wyld, 2010) and the Late Eocene Soebi Blanco suggest that these two

**Table 5**
U–Pb LA-ICP-MS analytical and age results from the analyzed sandstones.

| Sample name | 238U 206Pb | 1 Sigma % error | 207 Pb 206 Pb | 1 Sigma % error | 206/238 age | 1 Sigma abs err | 207/206 age | 1 Sigma abs err | Best age | 1 Sigma abs err |
|---|---|---|---|---|---|---|---|---|---|---|
| 030223-1_100 | 6.062 | 1.85 | 0.0771 | 0.67% | 984.3 | 16.9 | 1123.1 | 13.3 | 1123 | 13 |
| 030223-1_99 | 5.368 | 1.06 | 0.0798 | 0.44 | 1101.2 | 10.8 | 1192.4 | 8.7 | 1192 | 8.7 |
| 030223-1_98 | 6.447 | 1.07 | 0.0743 | 0.59 | 929.5 | 9.3 | 1050.7 | 11.8 | 930 | 9.3 |
| 030223-1_97 | 9.942 | 1.58 | 0.0674 | 0.99 | 617.8 | 9.3 | 848.8 | 20.5 | 618 | 9.3 |
| 030223-1_96 | 11.38 | 1.11 | 0.0571 | 0.79 | 543.1 | 5.8 | 496.7 | 17.4 | 543 | 5.8 |
| 030223-1_95 | 7.227 | 1.17 | 0.0698 | 0.83 | 835.5 | 9.2 | 922.1 | 16.9 | 836 | 9.2 |
| 030223-1_94 | 6.495 | 1.80 | 0.0767 | 0.79 | 923.2 | 15.5 | 1112.5 | 15.7 | 1113 | 16 |
| 030223-1_93 | 7.634 | 1.29 | 0.0692 | 0.79 | 793.5 | 9.6 | 904.9 | 16.3 | 794 | 9.6 |
| 030223-1_92 | 8.039 | 1.24 | 0.0726 | 0.46 | 755.8 | 8.8 | 1003.7 | 9.3 | 756 | 8.8 |
| 030223-1_91 | 6.312 | 1.69 | 0.0749 | 0.92 | 948 | 14.9 | 1066.3 | 18.4 | 1066 | 18 |
| 030223-1_90 | 8.335 | 1.99 | 0.0777 | 0.61 | 730.4 | 13.7 | 1139.3 | 12 | 730 | 14 |
| 030223-1_89 | 29.92 | 1.32 | 0.052 | 1.15 | 212 | 2.7 | 287.6 | 26 | 212 | 2.7 |
| 030223-1_88 | 7.374 | 1.83 | 0.0715 | 1.52 | 819.8 | 14.1 | 972.7 | 30.7 | 820 | 14 |
| 030223-1_87 | 8.583 | 1.32 | 0.0721 | 0.56 | 710.4 | 8.9 | 987.7 | 11.3 | 710 | 8.9 |
| 030223-1_86 | 11.66 | 1.97 | 0.0569 | 1.85 | 530.2 | 10 | 488.9 | 40.3 | 530 | 10 |
| 030223-1_85 | 3.822 | 2.17 | 0.0959 | 0.42 | 1498.3 | 28.9 | 1545.4 | 8 | 1545 | 8.0 |
| 030223-1_84 | 6.844 | 1.53 | 0.0763 | 0.60 | 879.2 | 12.5 | 1103.2 | 11.9 | 879 | 13 |
| 030223-1_83 | 3.690 | 1.55 | 0.0988 | 0.57 | 1545.9 | 21.3 | 1602.4 | 10.5 | 1602 | 11 |
| 030223-1_82 | 6.330 | 1.46 | 0.0733 | 0.52 | 945.6 | 12.8 | 1021.6 | 10.4 | 946 | 13 |
| 030223-1_81 | 4.500 | 1.99 | 0.0874 | 0.89 | 1293.5 | 23.3 | 1368.6 | 17.1 | 1369 | 17 |
| 030223-1_80 | 8.099 | 2.23 | 0.0663 | 1.03 | 750.6 | 15.8 | 816.3 | 21.4 | 751 | 16 |
| 030223-1_79 | 8.604 | 2.21 | 0.0648 | 1.01 | 708.8 | 14.8 | 766.4 | 21.1 | 709 | 15 |
| 030223-1_78 | 5.694 | 1.94 | 0.0782 | 0.58 | 1043 | 18.7 | 1152.7 | 11.5 | 1153 | 11 |
| 030223-1_77 | 6.717 | 2.58 | 0.0794 | 0.62 | 894.6 | 21.5 | 1182 | 12.2 | 1182 | 12 |
| 030223-1_76 | 3.140 | 1.85 | 0.1238 | 0.30 | 1782.4 | 28.7 | 2011.2 | 5.3 | 2011 | 5.3 |
| 030223-1_75 | 5.035 | 1.94 | 0.0826 | 0.39 | 1167.8 | 20.7 | 1258.9 | 7.7 | 1259 | 7.7 |
| 030223-1_74 | 5.393 | 3.02 | 0.0812 | 0.33 | 1096.6 | 30.4 | 1226.6 | 6.5 | 1227 | 6.5 |
| 030223-1_73 | 7.936 | 6.53 | 0.071 | 0.42 | 765 | 47 | 956.6 | 8.5 | 765 | 47 |
| 030223-1_72 | 6.645 | 2.02 | 0.0724 | 0.73 | 903.7 | 17 | 996.8 | 14.8 | 904 | 17 |
| 030223-1_71 | 4.721 | 2.07 | 0.0853 | 0.47 | 1238.5 | 23.3 | 1321.3 | 9 | 1321 | 9.0 |
| 030223-1_70 | 5.248 | 1.98 | 0.0796 | 0.64 | 1124.5 | 20.4 | 1188.1 | 12.5 | 1188 | 12.5 |
| 030223-1_69 | 27.87 | 2.18 | 0.051 | 0.72 | 227.2 | 4.9 | 240 | 16.6 | 227 | 4.9 |
| 030223-1_68 | 24.47 | 2.13 | 0.0523 | 1.12 | 258.2 | 5.4 | 298.5 | 25.4 | 258 | 5.4 |
| 030223-1_67 | 2.523 | 2.15 | 0.1733 | 0.40 | 2152.4 | 39.2 | 2590 | 6.6 | 2590 | 6.6 |
| 030223-1_66 | 5.233 | 2.11 | 0.0779 | 0.41 | 1127.3 | 21.8 | 1145.3 | 8.1 | 1145 | 8.1 |
| 030223-1_65 | 12.09 | 2.04 | 0.0588 | 0.80 | 512.3 | 10.1 | 560 | 17.4 | 512 | 10 |
| 030223-1_64 | 7.035 | 6.17 | 0.1126 | 4.54 | 856.8 | 49.3 | 1842.6 | 79.9 | 1843 | 80 |
| 030223-1_63 | 6.959 | 1.91 | 0.0698 | 0.43 | 865.5 | 15.4 | 921.2 | 8.7 | 866 | 15 |
| 030223-1_62 | 3.916 | 2.04 | 0.0986 | 0.41 | 1466 | 26.7 | 1598.6 | 7.6 | 1599 | 7.6 |
| 030223-1_61 | 3.859 | 2.11 | 0.0973 | 0.73 | 1485.5 | 27.9 | 1572.2 | 13.5 | 1572 | 14 |
| 030223-1_60 | 6.582 | 1.87 | 0.0706 | 0.62 | 911.7 | 15.9 | 946.1 | 12.7 | 912 | 16 |
| 030223-1_59 | 7.016 | 2.08 | 0.0711 | 0.80 | 859 | 16.7 | 960.9 | 16.2 | 859 | 17 |
| 030223-1_58 | 5.075 | 1.92 | 0.0814 | 0.61 | 1159.4 | 20.4 | 1231.7 | 11.9 | 1232 | 12 |
| 030223-1_57 | 10.22 | 2.00 | 0.0602 | 0.80 | 601.7 | 11.5 | 612.1 | 17.3 | 602 | 11 |
| 030223-1_56 | 6.044 | 2.07 | 0.0761 | 0.84 | 987.1 | 18.9 | 1098.2 | 16.8 | 1098 | 17 |
| 030223-1_55 | 34.51 | 3.18 | 0.0504 | 3.48 | 184.1 | 5.8 | 214.5 | 78.6 | 184 | 5.8 |
| 030223-1_54 | 6.755 | 2.32 | 0.0732 | 1.28 | 890 | 19.2 | 1019.4 | 25.7 | 890 | 19 |
| 030223-1_53 | 7.694 | 2.25 | 0.0771 | 0.85 | 787.7 | 16.7 | 1122.8 | 16.8 | 788 | 17 |
| 030223-1_52 | 5.165 | 1.88 | 0.0789 | 0.57 | 1140.9 | 19.7 | 1169.4 | 11.2 | 1169 | 11 |
| 030223-1_51 | 6.090 | 2.09 | 0.077 | 0.67 | 980.1 | 19 | 1122.2 | 13.3 | 1122 | 13 |
| 030223-1_50 | 5.171 | 2.29 | 0.079 | 1.06 | 1139.7 | 23.9 | 1171.3 | 20.8 | 1171 | 21 |
| 030223-1_49 | 23.49 | 2.04 | 0.0519 | 1.21 | 268.8 | 5.4 | 281.4 | 27.4 | 269 | 5.4 |
| 030223-1_48 | 24.35 | 2.04 | 0.0515 | 1.28 | 259.5 | 5.2 | 263.5 | 29.1 | 260 | 5.2 |
| 030223-1_47 | 6.695 | 1.94 | 0.0731 | 0.65 | 897.5 | 16.2 | 1016.2 | 13.1 | 898 | 16 |
| 030223-1_46 | 6.570 | 2.30 | 0.0756 | 1.26 | 913.3 | 19.6 | 1085.7 | 25 | 913 | 20 |
| 030223-1_45 | 90.85 | 2.48 | 0.0496 | 2.53 | 70.6 | 1.7 | 175.3 | 58 | 71 | 1.7 |
| 030223-1_44 | 6.698 | 2.05 | 0.07 | 0.75 | 897.1 | 17.2 | 927.9 | 15.3 | 897 | 17 |
| 030223-1_43 | 6.052 | 2.05 | 0.0766 | 0.72 | 985.8 | 18.7 | 1110.7 | 14.4 | 986 | 19 |
| 030223-1_42 | 5.838 | 1.92 | 0.0742 | 0.55 | 1019.2 | 18.1 | 1047.9 | 11 | 1048 | 11 |
| 030223-1_41 | 5.835 | 2.01 | 0.0772 | 0.58 | 1019.8 | 18.9 | 1125.5 | 11.5 | 1126 | 12 |
| 030223-1_40 | 6.254 | 1.66 | 0.073 | 0.80 | 956.3 | 14.7 | 1014.5 | 16.1 | 956 | 15 |
| 030223-1_39 | 4.464 | 1.65 | 0.0811 | 0.83 | 1303.1 | 19.4 | 1222.7 | 16.3 | 1303 | 19 |
| 030223-1_38 | 6.042 | 2.01 | 0.0743 | 1.15 | 987.3 | 18.4 | 1049.3 | 23 | 1049 | 23 |
| 030223-1_37 | 6.081 | 1.59 | 0.0727 | 0.58 | 981.5 | 14.5 | 1006.7 | 11.6 | 982 | 14 |
| 030223-1_36 | 5.195 | 1.71 | 0.0787 | 0.92 | 1134.8 | 17.7 | 1164.7 | 18.2 | 1165 | 18 |
| 030223-1_35 | 6.744 | 1.76 | 0.0697 | 0.91 | 891.3 | 14.6 | 918.1 | 18.6 | 891 | 15 |
| 030223-1_34 | 5.807 | 1.72 | 0.0723 | 0.85 | 1024.2 | 16.3 | 995.1 | 17.2 | 995 | 17 |
| 030223-1_33 | 6.684 | 1.71 | 0.0691 | 0.76 | 898.7 | 14.3 | 903.2 | 15.5 | 899 | 14 |
| 030223-1_32 | 5.151 | 1.51 | 0.079 | 0.54 | 1143.7 | 15.8 | 1171.7 | 10.6 | 1172 | 11 |
| 030223-1_31 | 5.596 | 1.74 | 0.08 | 0.54 | 1059.9 | 17 | 1196.2 | 10.5 | 1196 | 11 |
| 030223-1_30 | 2.802 | 1.55 | 0.1293 | 0.54 | 1967.5 | 26.3 | 2087.8 | 9.5 | 2088 | 9.5 |
| 030223-1_29 | 5.798 | 1.60 | 0.0791 | 0.50 | 1025.7 | 15.1 | 1174.7 | 9.9 | 1175 | 9.9 |
| 030223-1_28 | 2.528 | 1.59 | 0.1377 | 0.57 | 2148.4 | 29 | 2198.2 | 9.9 | 2198 | 9.9 |

(*continued on next page*)

**Table 5** (*continued*)

| Sample name | 238U 206Pb | 1 Sigma % error | 207 Pb 206 Pb | 1 Sigma % error | 206/238 age | 1 Sigma abs err | 207/206 age | 1 Sigma abs err | Best age | 1 Sigma abs err |
|---|---|---|---|---|---|---|---|---|---|---|
| 030223-1_27 | 4.490 | 2.00 | 0.0959 | 0.52 | 1296.3 | 23.4 | 1544.8 | 9.8 | 1545 | 9.8 |
| 030223-1_26 | 3.538 | 1.72 | 0.105 | 0.55 | 1604.5 | 24.4 | 1713.7 | 10.1 | 1714 | 10 |
| 030223-1_25 | 24.43 | 2.04 | 0.0569 | 1.62 | 258.6 | 5.2 | 487.9 | 35.5 | 259 | 5.2 |
| 030223-1_24 | 5.967 | 2.30 | 0.0774 | 0.80 | 998.8 | 21.2 | 1131.7 | 15.9 | 1132 | 15.9 |
| 030223-1_23 | 6.046 | 1.92 | 0.0733 | 0.81 | 986.7 | 17.6 | 1023.6 | 16.4 | 1024 | 16.4 |
| 030223-1_22 | 24.73 | 2.53 | 0.0535 | 1.27 | 255.5 | 6.3 | 352.1 | 28.5 | 256 | 6.3 |
| 030223-1_21 | 5.560 | 2.15 | 0.0779 | 1.01 | 1066.2 | 21.1 | 1144.9 | 19.9 | 1145 | 20 |
| 030223-1_20 | 5.075 | 2.31 | 0.0805 | 0.47 | 1159.5 | 24.5 | 1209.8 | 9.2 | 1210 | 9.2 |
| 030223-1_19 | 4.842 | 3.29 | 0.081 | 0.70 | 1210.2 | 36.2 | 1220.4 | 13.8 | 1220 | 13.8 |
| 030223-1_18 | 90.92 | 3.43 | 0.0485 | 3.83 | 70.5 | 2.4 | 121.9 | 87.9 | 70.5 | 2.4 |
| 030223-1_17 | 5.680 | 2.51 | 0.0794 | 0.53 | 1045.5 | 24.2 | 1183 | 10.4 | 1183 | 10 |
| 030223-1_16 | 7.580 | 2.66 | 0.0714 | 1.06 | 798.8 | 20 | 968.9 | 21.4 | 799 | 20 |
| 030223-1_15 | 3.882 | 3.30 | 0.0998 | 1.05 | 1477.7 | 43.4 | 1620.1 | 19.5 | 1620 | 19 |
| 030223-1_14 | 6.521 | 2.20 | 0.0705 | 0.74 | 919.8 | 18.9 | 943.1 | 15.1 | 920 | 19 |
| 030223-1_13 | 11.63 | 2.40 | 0.0599 | 1.32 | 531.6 | 12.2 | 601.2 | 28.2 | 532 | 12 |
| 030223-1_12 | 5.950 | 2.34 | 0.0795 | 0.49 | 1001.4 | 21.6 | 1184.3 | 9.7 | 1184 | 10 |
| 030223-1_11 | 7.170 | 2.25 | 0.0696 | 0.57 | 841.6 | 17.7 | 916 | 11.6 | 842 | 18 |
| 030223-1_10 | 91.51 | 2.63 | 0.0481 | 2.58 | 70.1 | 1.8 | 102.7 | 59.8 | 70 | 1.8 |
| 030223-1_9 | 4.792 | 2.21 | 0.0889 | 0.54 | 1221.8 | 24.5 | 1402 | 10.4 | 1402 | 10 |
| 030223-1_8 | 24.20 | 2.36 | 0.052 | 1.30 | 261 | 6 | 283.7 | 29.4 | 261 | 6.0 |
| 030223-1_7 | 5.831 | 2.36 | 0.0782 | 0.44 | 1020.4 | 22.3 | 1151.6 | 8.7 | 1152 | 8.7 |
| 030223-1_6 | 6.791 | 2.23 | 0.0709 | 0.90 | 885.6 | 18.4 | 953.5 | 18.2 | 886 | 18 |
| 030223-1_5 | 5.193 | 2.19 | 0.0807 | 0.67 | 1135.2 | 22.7 | 1214.2 | 13.1 | 1214 | 13 |
| 030223-1_4 | 5.069 | 2.30 | 0.0809 | 0.59 | 1160.8 | 24.4 | 1220.1 | 11.5 | 1220 | 12 |
| 030223-1_3 | 11.72 | 2.28 | 0.0605 | 0.52 | 528 | 11.5 | 619.9 | 11.2 | 528 | 12 |
| 030223-1_2 | 11.29 | 2.32 | 0.0582 | 1.13 | 547.3 | 12.2 | 537.4 | 24.4 | 547 | 12 |
| 030223-1_1 | 4.081 | 2.62 | 0.0871 | 0.56 | 1412.8 | 33.1 | 1363.1 | 10.7 | 1363 | 11 |

blocks make part of a coherent Early Paleogene orogen that extend along the northern Andes and the Caribbean that record the initial interaction of the advancing front in the Caribbean plate with the South American margin in the Late Cretaceous (Lugo and Mann, 1995; Pindell et al., 1998, 2005; Bayona et al., 2011; Cardona et al., 2011; Villagomez et al., 2011).

Following this event a new subduction zone was started in the continental margin and oblique convergence was installed and the Caribbean plate front and continue its migration to the east, forming arc-continent orogeny and subsequently allowing the installation of a subduction zone. By ca. 58–50 Ma the subduction of the Caribbean plate under the South American margin was responsible for the built of a magmatic arc, represented by several intermediate plutons in the Guajira region and the southern Sierra Nevada de Santa Marta (Cardona et al., 2011; Bayona et al., 2012). And arc-continent collision was already accomplished in the adjacent Falcon region as recorded by the emplacement of the Lara Nappes (Baquero et al., 2009; Escalona and Mann, 2010).

In the Late Eocene oblique convergence continues, the margin experienced transtension with basin growth as recorded in the 400 m fluvial sedimentation and the apparently fast marine transgression represented by the overlying carbonates (Pijpers, 1933; Beets et al., 1977) of the Soebi Blanco Formation, that together suggest high accommodation space and basin instability. A similar scenario is recorded in the adjacent Falcon basin where strong subsidence has been documented (Baquero et al., 2009; Quiroz and Jaramillo, 2010).

**Table 6**
U–Th/He thermochronology age results from the analyzed sandstones.

| Sample name | ppm U | ppm Th | nmol 4He/g | Date (Ma) | 1 Sigma error (Ma) |
|---|---|---|---|---|---|
| 030223-3_Zr1 | 466.8 | 31.21 | 115.5 | 57.57 | 0.85 |
| 030223-3_Zr2 | 1552 | 218.5 | 423.2 | 61.98 | 0.90 |
| 030222-1_Zr1 | 94.2 | 33.35 | 23.42 | 50.13 | 0.70 |
| 030222-1_Zr2 | 177.0 | 75.84 | 47.69 | 51.72 | 0.71 |
| 030222-12_Zr4 | 243.8 | 74.66 | 63.31 | 54.98 | 0.77 |
| 030222-1_Zr3 | 98.4 | 52.87 | 142.9 | 306.5 | 4.23 |
| 030223-2_Zr1 | 471.2 | 70.38 | 122.9 | 64.98 | 0.94 |
| 030223-2_Zr2 | 478.8 | 62.36 | 124.7 | 63.05 | 0.92 |
| 030223-2_Zr3 | 896.7 | 59.68 | 215.7 | 64.21 | 0.94 |

Provenance from the Late Eocene units in northern South America including the Maracaibo, Guajira and Catatumbo-Cesar-Rancheria shows the existence of at least two contrasting patterns: a southeastern that include the Maracaibo and Catatumbo-Cesar-Rancheria (Fig. 6D and E) characterized by significant >1000 Ma age populations and a Guajira + Bonaire signature where this peak is not so representative and Grenvillian Sources are characteristics (Zapata et al., 2010; Xie et al., 2010 and Ayala et al., 2012, Fig. 6–C). Such provincialism indicates that northern South America was characterized by different drainage systems in the Late Eocene and the existence of different basin-uplift systems. The Maracaibo, Catatumbo and Cesar-Rancheria recording the denudation of the main Andes and the Guajira, Leeward Antilles and probably the Falcon Basin (Quiroz et al., 2012) related to more local basin-uplift systems.

It is therefore suggested that the formation of a transtensional setting in northern South America since the Middle Eocene, is responsible for basin formation along-strike of the Leeward Antilles from the SABM and major block rotation (Macdonald and Opdyke, 1972; Muessig, 1984; Macellari, 1995; Gorney et al., 2007; Beardsley and Ave-Lallemant, 2007; Montes et al., 2010; Zapata et al., 2010; Escalona and Mann, 2010).

Regional-scale plate tectonic reconstructions suggest that the relative convergence between the Caribbean and South American margin changes from a ca. 56–38 Ma orthogonal convergence to 38–19.5 Ma oblique (southeast) relations (Müller et al., 1999). We suggest that these major changes can explain the former existence of a continuous SABM orogenic belt with the associated growth of the Eocene continental arc and the subsequent transition to transtensional basin formation and the lateral fragmentation of the

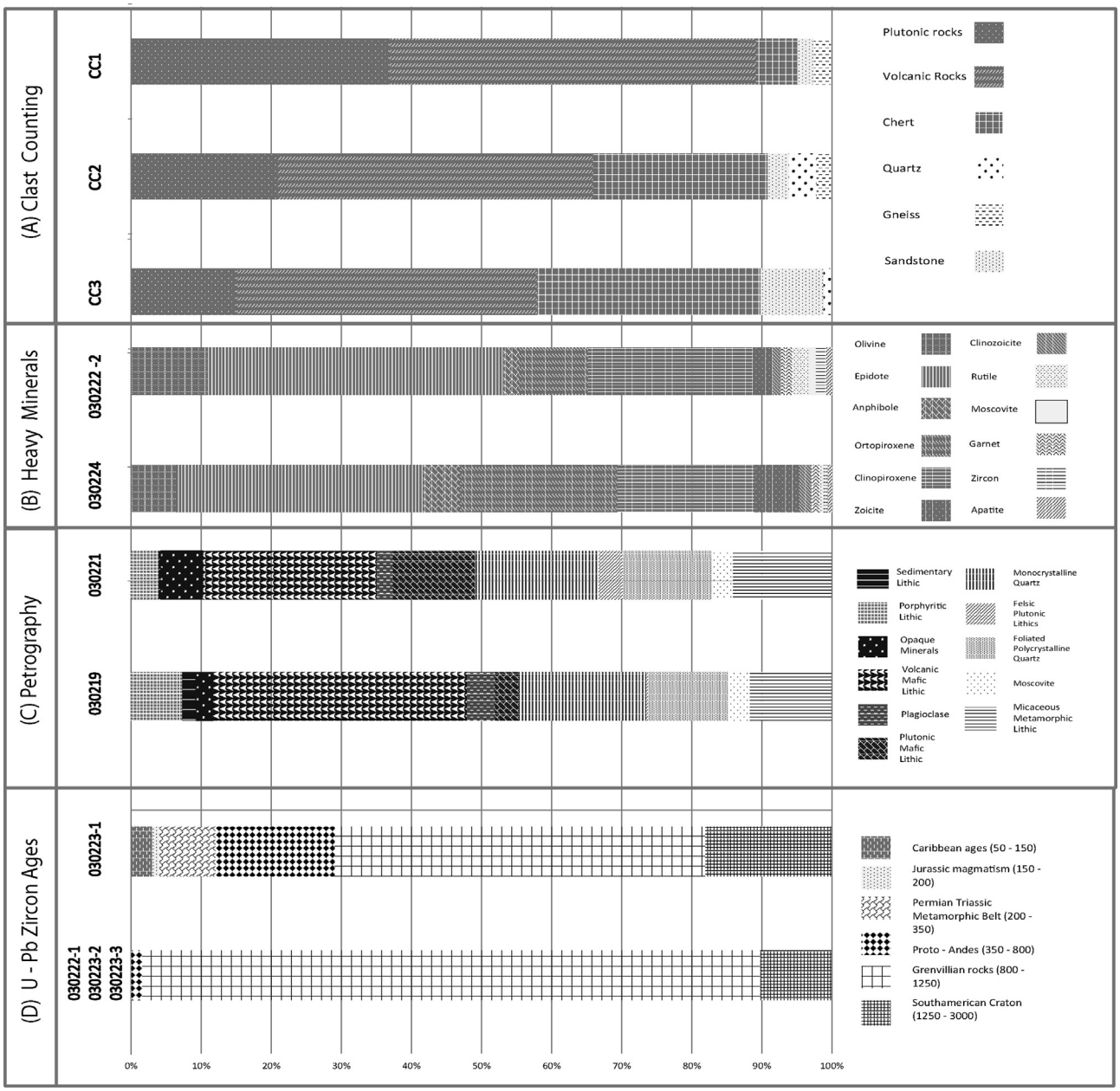


**Fig. 3.** Provenance analyses comparison and U–Pb ages from the metamorphic clasts. (A) Clast counting from Soebi Blanco conglomerates; (B) heavy minerals analyses from Soebi Blanco associated sandstones; (C) petrography from Soebi Blanco associated sandstones; (D) U–Pb zircon ages from associated sandstones and metamorphic clasts.

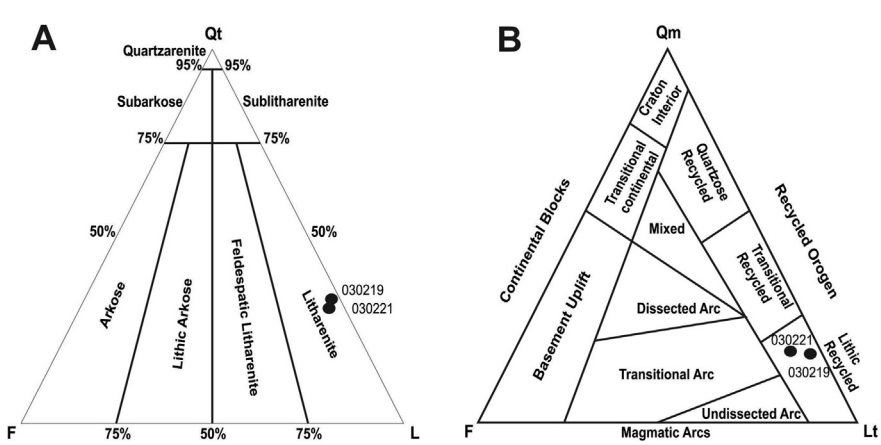


**Fig. 4.** (A). Sandstone classification after Folk (1980); and (B) sandstone provenance and tectonic setting (Dickinson, 1985).

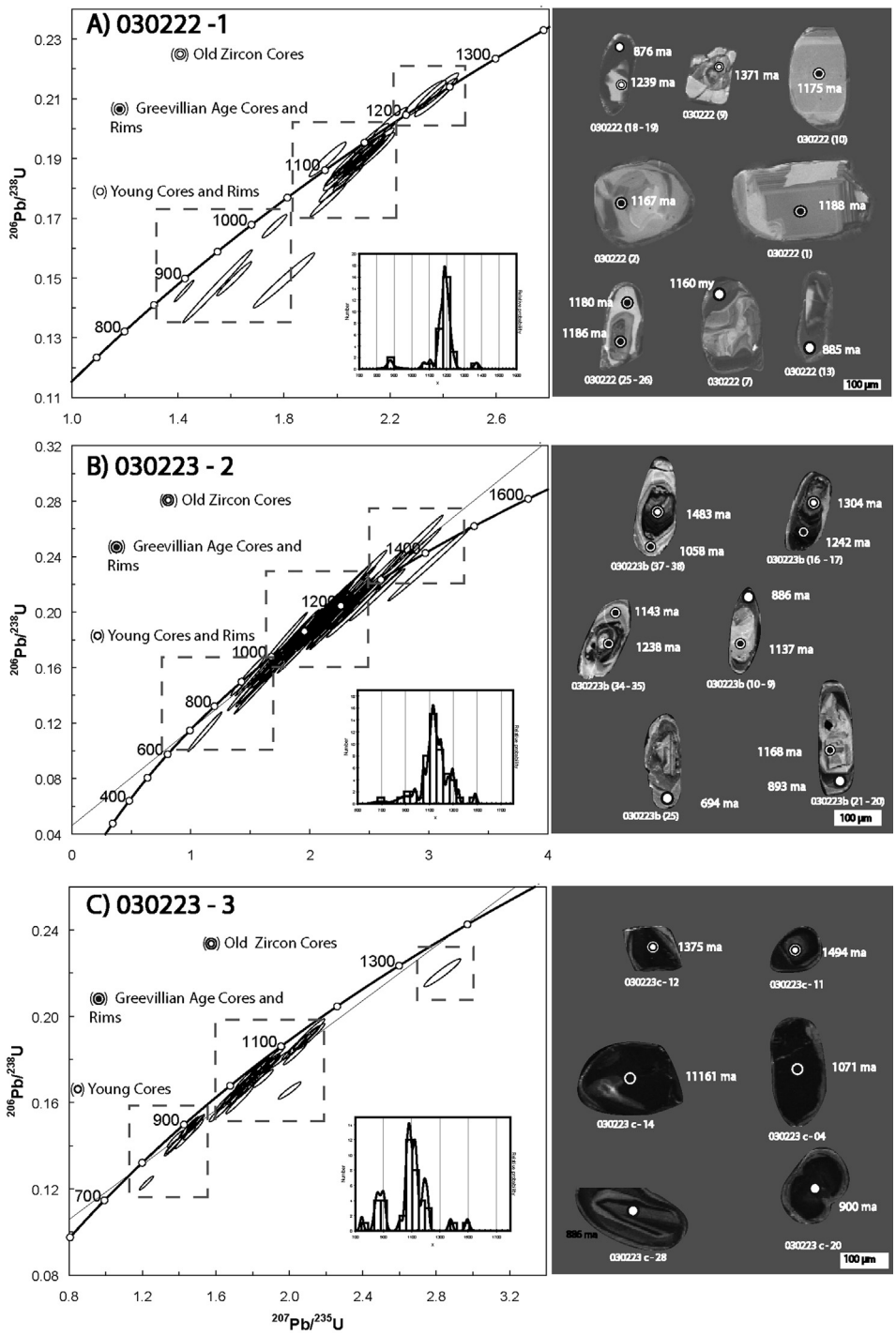


**Fig. 5.** U–Pb concordia diagrams from the analyzed metamorphic clasts and cathodoluminescence images from representative zircons.

continental margin as recorded in the Leeward Antilles and the Soebi Blanc accumulation.

Although our new results do not discriminate the two successive extensional stages seen in the Bonaire basin (Gorney et al., 2007), it is possible to suggest that the older Late Eocene–Oligocene is reflected by basement formation and the younger Oligo-Miocene event is reflected by the eastern lateral translation of the Leeward Antilles that may be also responsible for the huge accommodation style in the adjacent Falcon Basin (Quiroz and Jaramillo, 2010).

## 4. Conclusions

A maximum depositional age of ~50 Ma, was constrained using thermochronological ages obtained in metamorphic clasts from Soebi Blanco conglomerates.

The integrated provenance results from the Soebi Blanco Formation confirm a land connection between the Leeward Antilles and the SABM which is the most likely source for exotic clasts in Soebi Blanco gneissic and quartzose schist sources, implying transtensional basin formation and right-lateral displacement after

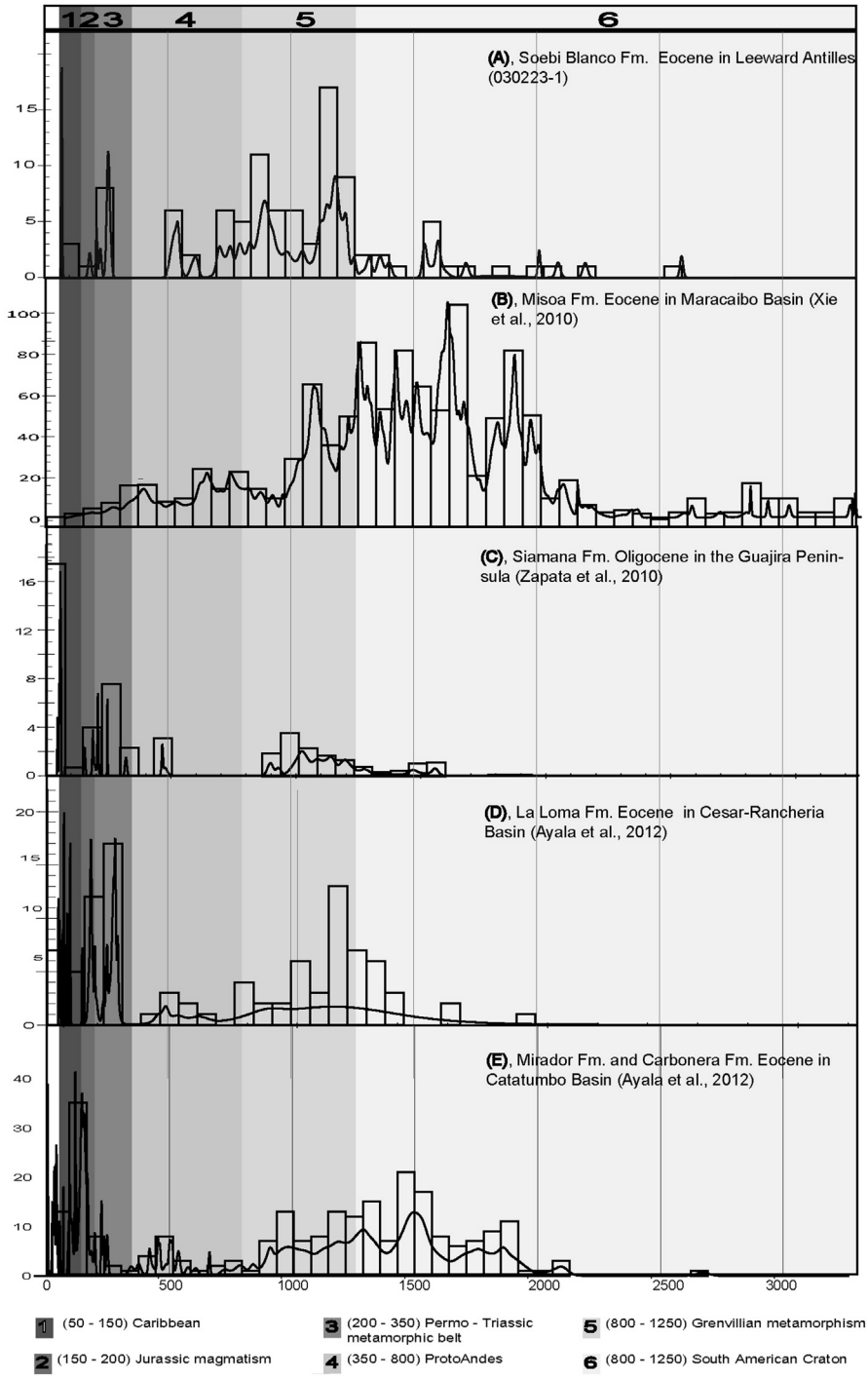


**Fig. 6.** U–Pb results from analyzed samples and other Caribbean provinces. (A) Detrital zircons from Soebi Blanco conglomerate matrix; (B) published data from the Eocene Misoa Formation in the Maracaibo basin (Xie et al., 2010); (C) published data from Oligocene conglomerates from Siamana Formation in the Guajira Peninsula; (D) published data from the Eocene La Loma Fm. In the Cesar-Rancheria Basin; and (E) published data from the Eocene Mirador Fm. and Carbonera Fm. in the Catatumbo Basin.

50 Ma due to the oblique convergence of the Caribbean and South American plates.

## Acknowledgments

We thank the Smithsonian Tropical Research Institute (STRI) and the environmental authorities of Bonaire for their support during several phases of the project. C. Jaramillo, Bayona, G., N. Hoyos, Londoño, L. and C. Echeverri are acknowledged for their discussions and continuous support. S. Zapata thanks COLCIENCIAS for its support as a young researchers fellowship. U. Ukchowdh, E. Abdel and G. Cañizalez helped with sample preparations and lab analyses. Finally we also thank the environmental authorities of Bonaire for their support and guidance.

## References

Ayala, R.C., Bayona, G., Cardona, A., Ojeda, C., Montenegro, O.C., Montes, C., Valencia, V., Jaramillo, C., 2012. The paleogene synorogenic succession in the northwestern Maracaibo block: tracking intraplate uplifts and changes in sediment delivery systems. J. South Am. Earth Sci. 39, 93–111.

Baquero, M., Acosta, J., Kassabji, E., Zamora, J., Sousa, J.C., Josmat, R., Gobras, J., Melo, L., Schneider, F., 2009. Polyphase development of the Falcón Basin in northwestern Venezuela: implications for oil generation. In: Geological Society of London, Special Publication, vol. 328, pp. 587–612.
Bayona, G., Montes, C., Cardona, A., Jaramillo, C., Ojeda, G., Valencia, V., Ayala-Calvo, C., 2011. Intraplate subsidence and basin filling adjacent to an oceanic arc-continent collision: a case from the southern Caribbean–South America plate margin. Basin Res. 10, 1365–2117.
Bayona, G., Cardona, A., Jaramillo, C., Montes, C., Valencia, V., Ayala-Calvo, C., Montenegro, O., Ibanez-Mejia, M., 2012. Early Paleogene magmatism in the Northern Andes: insights on the effects of the oceanic plateau–continent convergence. Earth Planet. Sci. Lett. 331–332, 97–111.
Beardsley, A.G., Ave-Lallemant, H.G., 2007. Oblique collision and accretion of the Netherlands Leeward Antilles to South America. Tectonics 26 (16).
Beets, D.J., 1972. Lithology and Stratigraphy of the Cretaceous and Danian succession of Curaçao. Ph.D thesis, p. 153 (Natuurwet, Studiekring Sur).
Beets, D.J., 1996. Geological Map of Aruba, Scale 1:25,000, in the Caribbean Region. Harlem, Netherlands.
Beets, D.J., MacGillavry, H., Klaver, G., 1977. Geology of the cretaceous and early tertiary of Bonaire. In: 8th Caribbean Geological Conference Guide to Field Excursions. GUA Paper of Geology, vol. 10, pp. 18–28.
Beets, D.J., Maresch, W.V., Klaver, A., Montana, R., Bocchio, R., Beunk, F.F., Moen, H.P., 1984. Magmatic rock series and high-pressure metamorphism as constraints on the tectonic history of the southern Caribbean, in the Caribbean–South American plate boundary and regional tectonics. Geol. Soc. Am. Bull. 162.
Burke, K., Cooper, C., Dewey, J.F., Mann, P., Pindell, I.L., 1984. Caribbean tectonics and relative plate motions. Geol. Soc. Am. Bull. 162, 31–59.
Cardona, A., Cordani, U., Macdonald, W., 2006. Tectonic correlations of pre-Mesozoic crust from the northern termination of the Colombian Andes, Caribbean region. J. South Am. Earth Sci. 21, 337–354.
Cardona, A., Valencia, V., Bayona, G., Jaramillo, C., Ojeda, G., Ruiz, J., 2009. U/Pb LA-MC-ICP-MS zircon geochronology and geochemistry from a post-collisional biotite granite of the Baja Guajira basin, Colombia: implications for Late Cretaceous and Neogene Caribbean–South America tectonics. J. Geol. 117, 685–692.
Cardona, A., Valencia, V., Bustamante, C., García-Casco, A., Ojeda, G., Ruiz, J., Saldarriaga, M., Weber, M., 2010b. Tectonomagmatic setting and provenance of the Santa Marta Schists, Northern Colombia: insights on the growth and approach of Cretaceous Caribbean oceanic terranes to the South American continent. J. South Am. Earth Sci. 29, 784–804.
Cardona, A., Valencia, V., Weber, M., Duque, J., Montes, C., Reiners, P., Domanik, K., Nicolescu, S., Villagomez, D., 2011. Transient Cenzoic tectonic stages in the southern margin of the Caribbean plate: U–Th/He thermochronological constraints from Eocene plutonic rocks in the Santa Marta Massif and Serranía de Jarara, northern Colombia. Geol. Acta 9, 445–466.
Cardona, A., Montes, C., Bayona, G., Jaramillo, C., Lopez, M., Silva, J., Valencia, V., Vanegas, J., Zapata, S., 2013. Timing and tectonic processes associated to the Late Cretaceous to Paleogene transition from collision to subduction in the northern margin of Colombia. In: AGU Meeting of the Americas.
Cardona, A., Valencia, V., Bayona, G., Duque, J., Ducea, M., Gehrels, G., Jaramillo, C., Montes, C., Ojeda, G., Ruiz, J., 2010a. Early-subduction-related orogeny in the northern Andes: Turonian to Eocene magmatic and provenance record in the Santa Marta Massif and Rancheria Basin, northern Colombia. Terra Nova. http://dx.doi.org/10.1111/j.1365-3121.2010.00979.x.
Chang, Z., Vervoort, J.D., McClelland, W.C., Knaack, C., 2006. U–Pb dating of zircon by LA-ICP-MS. Geochem. Geophys. Geosyst. 7, 1–14.
Cordani, U.G., Cardona, A., Jimenez, D., Liu, D., Nutman, A.P., 2005. Geochronology of Proterozoic basement inliers from the Colombian Andes: tectonic history of remmants from a fragmented Grenville Belt. In: Geological Society of London, Special Publications, pp. 329–346.
Cowan, D.S., 1982. Geological evidence for post-40 m.y. B.P. large-scale northwestward displacement of part of southeastern Alaska. Geology 6, 309–313.
Dickinson, W.R., 1985. Interpreting provenance relations from detrital modes of sandstones. Proven. Arenites 333–361.
Escalona, A., Mann, P., 2010. Tectonics, basin subsidence mechanisms, and paleogeography of the Caribbean–South American plate boundary zone. Mar. Petrol. Geol. 28, 8–39.
Farley, K.A., 2002. (U–Th)/He dating: techniques, calibrations, and applications. Rev. Mineral. Geochem. 47, 819–844.
Farley, K.A., Wolf, R.A., Silver, L.T., 1996. The effects of long alpha-stopping distances on (U– Th)/He ages. Geochim. Cosmochim. Acta 60, 4223–4229.
Ferguson, R., Hoey, T., Wathen, S., Werritty, A., 1996. Field evidence for rapid downstream fining of river gravels through selective transport. Geology 24, 179–182.
Fitzgerald, P.G., 2006. Interpretation of (U–Th)/He single grain ages from slowly cooled crustal terranes: a case study from the Transantarctic Mountains of Southern Victoria Land. Chem. Geol. 225, 91–120.
Folk, R.L., 1980. Petrology of Sedimentary Rocks. Hemphill, Austin, Texas, p. 182.
Fouke, B.W., Beets, C.J., Meyers, W.J., Hanson, G.N., Melillo, A.J., 1996. Chronoestratigraphy and dolomitization history of the Seroe Domi formation Curacao (Netherlands Antilles). Facies 35, 293–320.
Gabrielse, H., 1985. Major dextral transcurrent displacements along the Northern Rocky Mountain Trench and related lineaments in north-central British Columbia. Geol. Soc. Am. Bull. 95, 1–14.
Gehrels, G., Valencia, V., Pullen, A., 2006. Detrital zircon geochronology by laser-ablation multicollector ICPMS at the Arizona Laser Chron Center. Paleontol. Soc. Paper 12, 67–76.
Gonzalez de Juana, C., Arozena, J.A., Picard Cardillat, X. (Eds.), 1980. Geologia de Venezuela y sus Cuencas petroliferas. Caracas.
Gorney, D., Escalona, A., Mann, P., Magnani, M.B., 2007. Chronology of Cenozoic tectonic events in western Venezuela and the Leeward Antilles based on integration of offshore seismic reflection data and on-land geology. AAPG Bull. 91, 653–684.
Grande, S., Urbani, F., 2009. Presence of high-grade rocks in NW Venezuela of possible Grenvillian affinity. In: Geological Society of London, Special Publication, vol. 328, pp. 533–548.
Hargraves, R.B., Shagam, R., 1969. Paleomagnetic study of La Quinta Formation Venezuela. AAPG Bull. 53, 537–552.
Hourigan, J.K., Reiners, P., Brandon, M.T., 2005. U–Th zonation-dependent alpha-ejection in (U–Th)/He chronometry. Geochim. Cosmochim. Acta 69, 3349–3365.
Howard, J.L., 1993. The statistics of counting clasts in rudites: a review, with examples from the upper Palaeogene of southern California. Sedimentology 40, 157–174.
Jarrard, R.D., 1986. Terrane motion by strike-slip faulting of forearc slivers. Geology 14, 780–783.
Kerr, A.C., Tarney, J., Marriner, G.F., Nivia, A., Klaver, G., Saunders, A.D., 1996. The geochemistry and tectonic setting of late Cretaceous Caribbean and Colombian. J. South Am. Earth Sci. 9, 111–120.
Klaver, G., 1976. The Washikemba Formation, Bonaire. University of Utrecht, Netherlands.
Kodama, Y., 1994. Downstream changes in the lithology and grain size of fluvial gravels, the Watarase River, Japan: evidence of the role of abrasion in downstream fining. J. Sediment. Res. A64, 68–75.
Kosler, J., Sylvester, P., 2003. Present trends and the future of zircon in geochronology: laser ablation ICPMS. Rev. Mineral. Geochem. 53, 243–275.
Lockwood, J.P., 1965. Geology of the Serranía de Jarara area, Guajira Península, Colombia. Ph.D. thesis. Princeton University, p. 237.
Ludwig, K.C., 2007. User's Manual for Isoplot 3.7. Berkley Geochronology Center, Berkley, p. 70.
Lugo, J., Mann, P., 1995. Jurassic–Eocene tectonic evolution of Maracaibo Basin, in Venezuela. AAPG Bull., 699–725.
Macdonald, W., 1964. Geology of Serrania de Macuira Area, Guajira Peninsula, Colombia. Princeton University, N.J.
Macdonald, W.D., Opdyke, N.D., 1972. Tectonic rotations suggested by paleomagnetic results from northern Colombia, South America. J. Geophys. Res. 77, 5720–5730.
Macellari, C., 1995. Cenozoic sedimentation and tectonics of the southwestern Caribbean pull-apart basin, Venezuela and Colombia. AAPG Bull. 62, 757–780.
Mange, M.A., Maurer, H., 1991. Heavy Minerals in Colour. Springer-Verlag, p. 160.
Mendi, D., Baquero, M., Olivera, E., Urbano, F., Pinto, J., Grande, S., Valencia, V., 2013. Petrography and U–Pb zircon geochronology of geological units of the Mesa de Cocodite, Peninsula de Paraguana, Venezuela. In: AGU Meeting of the Americas.
Montes, C., Guzman, G., Bayona, G., Cardona, A., Valencia, V., 2010. Clockwise rotation of the Santa Marta massif and simultaneous Paleogene to Neogene deformation of the Plato-San Jorge and Cesar-Ranchería basins. J. South Am. Earth Sci. 29, 832–848.
Muessig, K., 1984. Structure and Cenozoic tectonics of the Falcon Basin, Venezuela, and adjacent areas. AAPG Bull. 62, 217–230.
Müller, R.D., Royer, J.Y., Cande, S.C., Roest, W.R., Maschenkov, S., 1999. Chapter 2 New constraints on the late cretaceous/tertiary plate tectonic evolution of the Caribbean. Sediment. Basins World 4, 33–59.
Neill, I., Kerr, A.C., Hastie, A., Stanek, K.P., Millar, I.L., 2011. Origin of the Aves Ridge and Dutch–Venezuelan Antilles: interaction of the Cretaceous 'Great Arc' and Caribbean–Colombian Oceanic Plateau? J. Geol. Soc. Lond. 168, 333–347.
Oldow, J.S., Bally, W.A., Hans, G., Lallemant, A., 1990. Transpression, orogenic float, and lithospheric balance. Geology 18, 991–994.
Pijpers, P.J., 1933. Geology and Paleontology of Bonaire. Geogr. Geol. Meded. Physiogr. Geol. Reeks. 8, 103.
Pindell, I.L., 2009. Tectonic evolution of the Gulf of Mexico, Caribbean and northern South America in the mantle reference frame: an update. In: Geological Society of London, Special Publication, vol. 328, pp. 1–56.
Pindell, I.L., Cande, S.C., Pitman Ille, W.C., Rowley, D.B., Dewey, J.F., LaBreque, J., Haxby, W., 1998. A plate kinematic framework for models of Caribbean evolution. Tectonophysics 155, 121–138.
Pindell, I.L., Kenan, L., Maresch, W.V., Stasnek, K.P., Draper, G., Higgs, R., 2005. Plate kinematic and crustal dynamics of circum-Caribbean arc-continent interactions: tectonic controls on basin development in the Proto-Caribbean margins. Geol. Soc. Am. Bull. 394, 7–52 (Special Paper).
Priem, H.N.A., 1979. K–Ar and Rb–Sr dating in the Cretaceous island arc succession of Bonaire, Netherlands Antilles. Geol. Mijnb. 58, 367–373.
Priem, H.N.A., Beets, D.J., Verdurmen, E.A.T., 1986. Precambrian in Early tertiary conglomerate on Bonaire, Netherland Antilles (Southern Caribbean Borderland): evidence for 300 km eastward displacement relative to South America mainland? Geol. Mijnb. 65, 35–40.
Quiroz, L., Jaramillo, C., 2010. Stratigraphy and sedimentary environments of Miocene shallow to marginal marine deposits in the Urumaco Trough, Falcon Basin, western Venezuela. In: Sanchez-Villagra, M., Aguilera, O., Carlini, A.A. (Eds.), Urumaco and Venezuelan Palaeontology. The Fossil Record of the Northern Neotropics. Indiana University Press, Bloomington, pp. 153–172.

Quiroz, L.I., Buatois, L.A., Mangano, M.G., Cardona, A., Montes, C., Silva-Tamayo, J.C., Vallejo, M.C., 2012. Miocene deltaic sedimentation in the Falcon Basin and its relation to climate and Caribbean tectonics. In: Cordilleran Section – 108th Annual Meeting (29–31 March). Geological Society of America.

Reiners, P., 2005. Zircon (U–Th)/He thermochronometry. In: Reiners, P.W., Ehlers, T.A. (Eds.), Thermochronology. Rev. Mineral. Geochem. vol. 58, 151–176.

Sinton, C.W., Duncan, R., Storey, M., Lewis, J., Estrada, J., 1998. An oceanic flood basalt province within the Caribbean Plate. Earth Planet Space 155, 221–235.

Sisson, V., 2008. Correlation of Eocene–Oligocene exhumation around the caribbean: Venezuela, Dominican Republic, Honduras, and Guatemala. In: Joint Meeting of the Geological Society of America, Edited, Houston.

Spikings, R., Winkler, W., Seward, D., Handler, R., 2001. Along-strike variations in the thermal and tectonic response of the continental Ecuadorian Andes to the collision with heterogeneous oceanic crust. Earth Planet. Sci. Lett. 186, 57–73.

Spikings, R., Winkler, W., Hughes, R.A., Handler, R., 2005. Thermochronology of allochthonous Terranes in Ecuador: unraveling the accretionary and post-accretionary history of the Northern Andes. Tectonophysics 399, 195–220.

Stearns, C., Mauk, F., Van der Voo, R., 1982. Late cretaceous – early tertiary paleomagnetism of Aruba and bonaire (Netherlands leeward antilles). J. Geophys. Res. 87, 1127–1141.

Thompson, P.M.E., Kempton, P.D., White, R.V., Saunders, A.D., Kerr, A.C., Tarney, J., Pringle, M.S., 2004. Elemental, Hf–Nd isotopic and geochronological constraints 938 on an island arc sequence associated with the Cretaceous Caribbean plateau: Bonaire, 939 Dutch Antilles. Lithos 74, 91–116.

Tschanz, C., Marvin, R., Cruz, J., Mehnert, H., Cebula, G., 1974. Geologic evolution of the Sierra Nevada de Santa Marta, Northeastern Colombia. Geol. Soc. Am. Bull. 85, 273–284.

Umhoefer, P.J., 1987. Northward translation of "BAJA British Columbia" along the Late Cretaceous to Paleocene margin of western North America. Tectonics 6, 377–394.

Valencia, V., Ruiz, J., Barra, F., Gehrels, G., Ducea, M., Titley, S.R., Ochoa, L., 2005. U–Pb zircon and Re–Os molybdenite geochronology from La Caridad porphyry copper deposit: insights for the duration of magmatism and mineralization in the Nacozari District, Sonora, Mexico. Miner. Deposita 40, 175–191.

Vallejo, C., Spikings, R., Winkler, W., Luzieux, L., Chew, D., Page, L., 2006. The early interaction between the Caribbean Plateau and the NW South American plate. Terra Nova 18, 264–269.

Van der Lelij, R., Spikings, R., Kerr, A.C., Kounov, A., Cosca, M., Chew, D., Villagomez, D., 2010. Thermochronology and tectonics of the leeward antilles: evolution of the southern caribbean plate boundary zone. Tectonics 29, 1–30.

Vence, E., 2008. Subsurface Structure, Stratigraphy, and Regional Tectonic Controls of the Guajira Margin of Northern Colombia. University of Austin Texas, p. 142.

Villagomez, D., Spikings, R., Magna, T., Kammer, A., Winkler, W., Beltrán, A., 2011. Geochronology, geochemistry and tectonic evolution of the Western and Central cordilleras of Colombia. Lithos 125, 875–896.

Weber, M., Cardona, A., Paniagua, F., Cordani, U., Sepúlveda, L., Wilson, R., 2009. The Cabo de la Vela mafic-ultramafic complex, Northeastern Colombian Caribbean region – a record of multi stage evolution of a Late Cretaceous intra-oceanic arc. In: Geological Society of London, Special Publication, vol. 394, pp. 549–568.

Weber, M., Cardona, A., Valencia, V., García-Casco, A., Tobón, M., Zapata, S., 2010. U/Pb detrital zircon provenance from Late Cretaceous metamorphic units of the Guajira Peninsula, Colombia: tectonic implications on the collision between the Caribbean arc and the South American margin. J. South Am. Earth Sci. 29, 805–816.

White, R.V., Tarney, J., Kerr, A.C., Saunders, A.D., Kempton, P.D., Pringle, M.S., Klaver, A., 1999. Modification of an oceanic plateau, Aruba, Dutch Caribbean: 964 implications for the generation of continental crust. Lithos 46, 43–68.

Wright, J.E., Wyld, S.J., 2010. Late Cretaceous subduction initiation on the 1 eastern margin of the Caribbean-2 Colombian oceanic plateau (CCOP): one Great Arc of the Caribbean (?). Geosphere 7, 468–493.

Xie, X.Y., Mann, P., Escalona, A., 2010. Regional provenance study of Eocene clastic sedimentary rocks within the South America–Caribbean plate boundary zone using detrital zircon geochronology. Earth Planet. Sci. Lett. 291, 159–171.

Zapata, S., Weber, M., Cardona, A., Valencia, V., Guzman, G., Tobón, M., 2010. Provenance of Oligocene conglomerates and associated sandstones from the Siamaná Formation, serranía de Jarara, Guajira, Colombia: implications for Oligocene Caribbean South American tectonics. Rev. Ciencias De. La Tierra 27, 7–24.